Western and Central Pacific Fisheries Commission

SCIENTIFIC COMMITTEE
TWENTIETH REGULAR SESSION

Manila, Philippines
14 – 21 August 2024

SEAPODYM:
Integration of new data to inform modelling of tuna's early life stages dynamics

WCPFC-SC20-2024/EB-IP-33
25 July 2024

Lucas Bonnin and Inna Senina[1]

[1] Oceanic Fisheries Programme, The Pacific Community

Contents

1 Executive summary

This information paper describes the integration of new data into the SEAPODYM model to inform early life stages of tuna species. So far, fisheries and tagging data were used to estimate SEAPODYM model parameters and predict tuna population dynamics and spatial structure. Such data is restricted to later life stages and may not enable to infer the location and timing of spawning and the dynamics of larvae and other early life stages. Here, alternative datasets, larval CPUE and spawning status of sampled adult females, are considered to inform early stages of tunas in the SEAPODYM model. A description of these datasets, the methods for using it in the SEAPODYM parameter estimation process, and their ability to improve current reference models in the Pacific Ocean, are described here. Focus is paid to two tuna species, a temperate species, albacore tuna (*Thunnus alalunga*), and a tropical species, yellowfin tuna (*Thunnus albacares*).

2 SEAPODYM model description

SEAPODYM is a mechanistical eulerian model that simulate tuna movements and population dynamics as a response to oceanic environment (ocean circulation, primary production, dissolved oxygen, water temperature). Parameters of this model are estimated using fisheries (catch, effort and length frequency) and tagging data. The model structure and parameter optimization process is described in I. Senina, Lehodey, et al. 2020 and its configuration for several tuna species were presented and updated in previous scientific reports (I. Senina, Hampton, et al. 2019, I. N. Senina et al. 2020).

3 Early life stage datasets

Two datasets able to inform modelling of tuna's early life stages dynamics were considered here: a digitized Japanese global larval CPUE dataset, hereafter called the Nishikawa dataset, and a gonad histological dataset collected by CSIRO for South Pacific albacore tuna.

3.1 The Nishikawa dataset

The Nishikawa dataset is the result of the largest survey of fish larvae to date, with a near-global extent and spanning over more than two decades (1956-1981; Nishikawa et al. 1985). A total of more than 63,000 tows of sampling nets over the Atlantic, Indian and Pacific Ocean (with main effort concentrated in the Western Pacific) was summarized over a 1° resolution grid, for 18 fish taxa, including four tuna species, yellowfin, albacore, skipjack (*Katsuwonus pelamis*) and bigeye tuna (*Thunnus obesus*). Yet, identification of fish larvae based on morphological criterion may have resulted in a confusion between yellowfin and bigeye tuna (Richards and Potthoff 1974). A more complete description of this dataset is available in Buenafe et al. 2022 and Nishikawa et al. 1985.

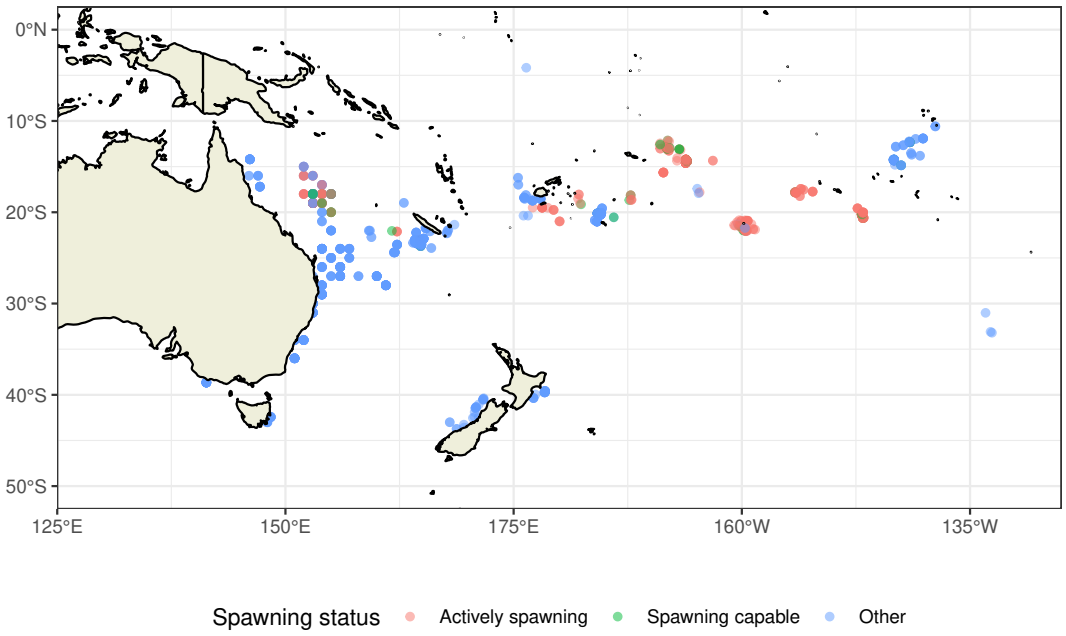

Figure 1: South Pacific albacore tuna female gonad sampling. Spawning status of sampled individuals were identified using histological analysis (Farley, A. J. Williams, et al. 2013).

This dataset was digitized from published Nishikawa atlas (Nishikawa et al. 1985) and made publicly available by Buenafe et al. 2022, providing larval CPUE aggregated at the seasonal scale (Jan-Mar, Apr-Jun, Jul-Sep, Oct-Dec) over a 1° resolution grid, and over unequal intervals of CPUE values. For example for yellowfin, larval CPUE is given as 0, 0-0.5, 0.5-1, 1-5 and >5 larvae per 1000 m^3 of water strained. Sampling effort was provided as values aggregated over unequal intervals of volume strained ($<$ 5, 5-20, 20-30, 30-50, $>$ 50 1000 m^3 of water strained).

3.2 The albacore female gonad histology dataset

This dataset was sampled, processed and analyzed by Farley, Hoyle, et al. 2014 and Farley, A. J. Williams, et al. 2013. Geo-referenced female gonad samples were collected on South Pacific albacore tuna between 2006 and 2011 and histological analysis was performed to identify maturity stage and spawning activity. This resulted in 1,177 gonad samples over the South Pacific (Figure 1), with spawning status classified as *Actively spawning* (321), *Spawning capable* (61), and *Other status* (795; *Immature, Developing, Regenerating, Regressed, Regressing*).

To use this type of data to inform the modelling of the early life stages dynamics in SEAPODYM, we first derived a seasonal spawning index on a longitude x latitude grid, calculated as the proportion of female gonads with positive spawning status. For this, we used *Actively spawning* females and those from the *Spawning capable* class, as these two classes were assessed to show similarity in both space and time (cf next paragraph). Second, it was necessary to identify the seasonal aggregation that allowed structure with

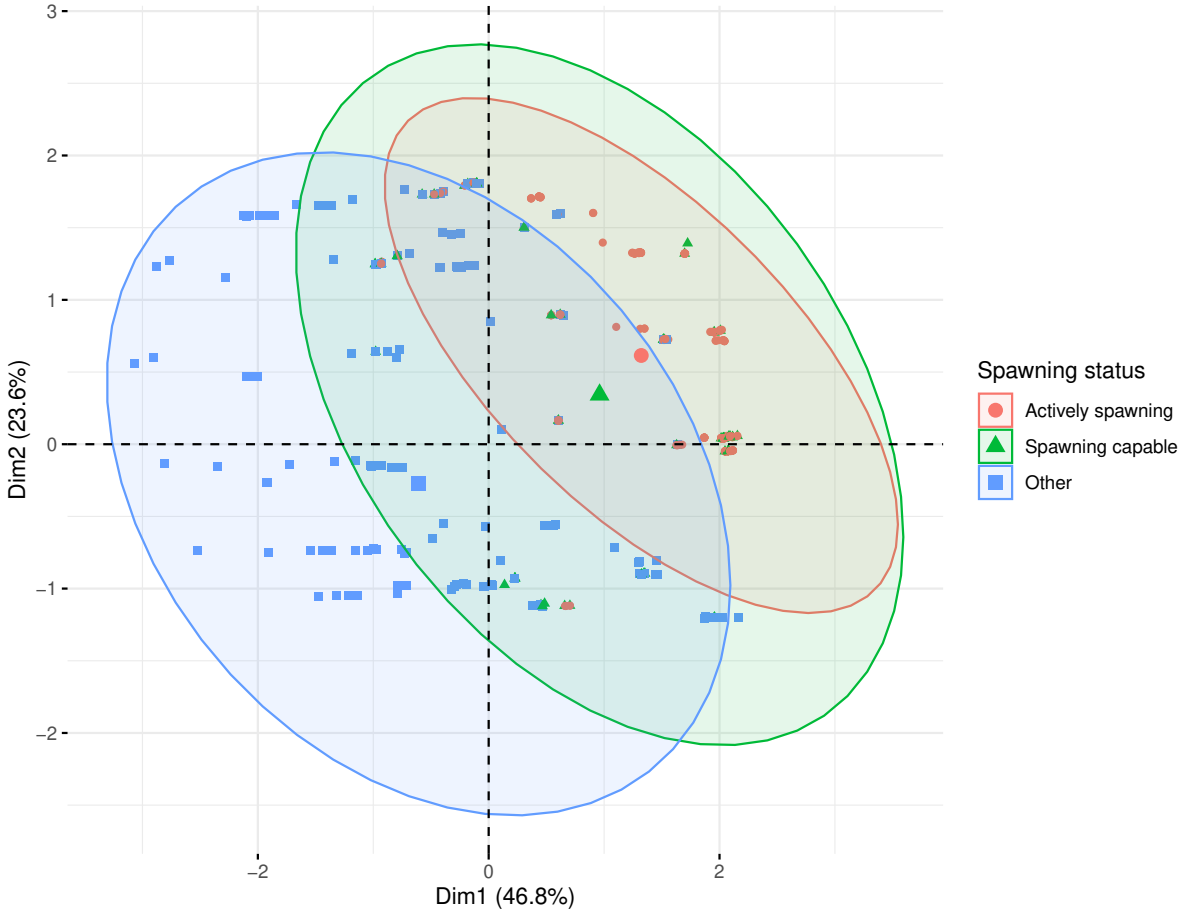

Figure 2: Principal Component Analysis: Distance between gonad samples in space and time. Projection of samples from a 4D-space (longitude, latitude, and cosinus- and sinus-transformed calendar month) to the plane presenting the largest variation in the data.

different spawning conditions, where each period could be considered homogeneous in terms of spawning status.

Samples were projected in a 4D-space consisting in standardized longitude, latitude and cosinus- and sinus-transformed calendar month using Principal Component Analysis, and between-samples euclidian distances were calculated. Transformation of calendar months was necessary to account for the cyclic nature of the variable, and both cosinus- and sinus- transformations ($\cos\left(\frac{2\pi \cdot \text{month}}{12}\right)$ and $\sin\left(\frac{2\pi \cdot \text{month}}{12}\right)$) were necessary to enable the unique projection of each calendar month. This revealed that *Spawning capable* samples were on average closer to *Actively spawning* samples than to *Other status* samples (Figure 2 and Table 1). Samples with *Spawning capable* status were thus classified as a positive spawning status and hence used to compute spawning index.

In order to identify the most pertinent seasonal aggregation of samples, the relationship between spawning status, calendar month and location was investigated using Recursive Partitioning, that finds optimal splitting rules to get homogeneous spawning status groups. Once again, calendar month was cosinus- and sinus-transformed to ac-

	Actively spawning	Spawning capable	Other
Actively spawning	1.78	2.09	3.09
Spawning capable		2.23	2.92
Other			2.38

Table 1: Average euclidian distance between samples from different spawning status groups.

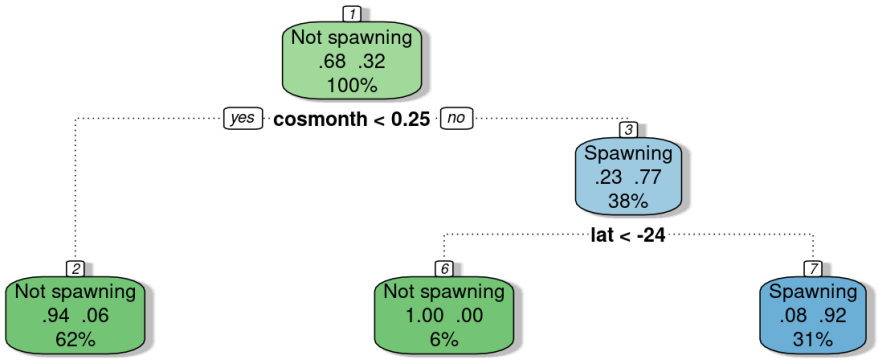

Figure 3: Hierarchical Partitioning of spawning status samples. Successive splitting on either longitude, latitude or cyclic transformation of calendar month was performed to obtain homogenous groups regarding spawning status. Graph generated using the *rattle* R package (G. Williams et al. 2022).

count for its cyclic nature. The *rpart* and *rattle* R packages (Therneau et al. 2023; G. Williams et al. 2022) were used for this analysis. Ten-fold cross-validation was used to identify the optimal tree complexity, beyond which growing the tree did not decrease relative error significantly (Supplementary Figure 19). This resulted in a simple partitioning rule based on $\cos\left(\frac{2\pi \cdot \text{month}}{12}\right)$ then latitude: positive spawning status samples were those with $\cos\left(\frac{2\pi \cdot \text{month}}{12}\right)$ greater than 0.25 (i.e. October to February) and above latitude 24°S (Figure 3). Consequently, samples were aggregated into two seasons, a 5-month spawning season between October and February, and a 7-month non-spawning season between March and September.

A seasonal spawning index was computed on a regular 2 x 2° grid used by SEAPODYM reference model of albacore tuna (I. N. Senina et al. 2020), as the proportion of positive spawning status samples in each grid cell during each season (Figure 11).

4 Implementation into SEAPODYM

4.1 Required implementions

Enabling the use of these new types of data in the SEAPODYM likelihoods required some new developments in the model computer code. First, the model predictions had to be

aggregated into seasons that are aligned with the observed variable. Second, we needed to define and implement an observation model, which transforms the model variable into observed variable. Third, to use the digitized Nishikawa dataset, we needed to establish and implement new likelihood functions that were suitable for categorical binned data.

4.2 Assimilation of continuous and categorical larvae data

The number of new recruits in SEAPODYM is the product of the Beverton-Holt stock-recruitment function and the spawning habitat index, as follows:

$$N(0) = H_s \cdot \frac{r \cdot N}{1 + b \cdot N}, \tag{1}$$

where $N(0)$ is the density of larvae that survived to the first age class, N the density of spawners, Hs the spawning habitat index, and r and b parameters of the Beverton-Holt function. The spawning habitat index Hs is defined as a function of surface temperature (SST), larvae prey density (Λ; proportional to primary productivity) and larvae predator density (F_1):

$$H_s = f_1(SST; T^*, \sigma) \cdot f_2(\Lambda; \alpha) \cdot f_3(F_1; \alpha_F, \beta_F) \tag{2}$$

where f_1, f_2 and f_3 functions are detailed in Supplementary Material Section 9.1.

Early life stages data can be used to inform either spawning habitat model, i.e. by fitting observed quantities to H_s, or to estimate parameters of the full population model, hence, fitting to $N(0)$. First of all, a linear scaling factor was introduced as a new parameter to scale model predictions to observations (thereafter called q_sp_larvae). When fitting predicted larval density to larval CPUE, this parameter plays the role of the sampling gear catchability of tuna larvae.

Cost function development

For continuous early life stages data, the negative logarithm of classic likelihood functions are already implemented: Poisson, Truncated Poisson, Zero-Inflated Poisson, Zero-Inflated Negative Binomial and Gaussian likelihood functions. Let X_{obs} be a continuous larval density observation and X_{pred} a continuous SEAPODYM model prediction. For example, the Poisson likelihood of this single observation is written as:

$$L(\theta|X_{obs}) = P_\theta(X = X_{obs}) = \frac{{X_{pred}}^{X_{obs}} e^{-X_{pred}}}{\Gamma(X_{obs} + 1)} \tag{3}$$

For categorical early life stage data, categorical equivalents of Poisson, Zero-Inflated Poisson, Negative Binomial and Zero-Inflated Negative Binomial likelihood functions were implemented. The likelihood of a model prediction to fall within a bin is calculated as the integral of the likelihood function between the bounds of the bins. Let X_{obs} be a

categorical larval density observation, with bounds X_{obs1} and X_{obs2}, and X_{pred} a continuous SEAPODYM model prediction. The Poisson likelihood of this single categorical observation is written as:

$$L(\theta|X_{obs}) = P_\theta(X_{obs1} < X < X_{obs2}) = \int_{X_{\text{obs1}}}^{X_{\text{obs2}}} \frac{{X_{pred}}^x e^{-X_{pred}}}{\Gamma(x+1)}\, dx \tag{4}$$

where the integral can be approximated numerically. For the last density category, a right-opened interval (e.g. > 5 larvae.1000 m^{-3}), a right bound was set to a large number to enable numerical approximation (here defined as 30).

Another type of likelihood, a mixed Gaussian Kernel, was also considered as an alternative formulation of the likelihood function for categorical data. It is defined as 1 when the model prediction falls with the observed bin, and following a Gaussian Kernel outside the bin:

$$L(\theta|X_{obs}) = \begin{cases} 1 & \text{if } X_{obs1} < X_{pred} < X_{obs2} \\ \frac{(X_{pred}-X_{obs1})^2}{2\sigma^2} & \text{if } X_{pred} < X_{obs1} \\ \frac{(X_{pred}-X_{obs2})^2}{2\sigma^2} & \text{if } X_{pred} > X_{obs2} \end{cases} \tag{5}$$

where σ is a parameter determining the width of the Gaussian Kernel. This function is illustrated in Figure 4.

Finally, the corresponding cost function used in function minimization is calculated as:

$$-lnL = -\sum_{obs} w \cdot \log\left(L(\theta|X_{obs})\right), \tag{6}$$

with

$$w = \begin{cases} 1 & \text{if } X_{obs} > 0 \\ w_0 & \text{if } X_{obs} = 0 \end{cases}, \tag{7}$$

where w_0 is the user-defined weighting factor for null observations ($0 \leq w_0 < 1$). The possibility to prevent or downweigh the fit to null observations was added to these functions to avoid interpreting null larvae as the true absence of larvae in a given grid cell.

For each of newly defined cost function, the adjoint code was written to provide exact analytical gradients to the quasi-Newton function minimization method.

5 Methods

5.1 Comparison of Nishikawa larval CPUE data to reference models

As Nishikawa data and reference model outputs were available on different spatial grids (1 x 1° and 2 x 2° grids resp.), comparison first required Nishikawa data to be degraded to

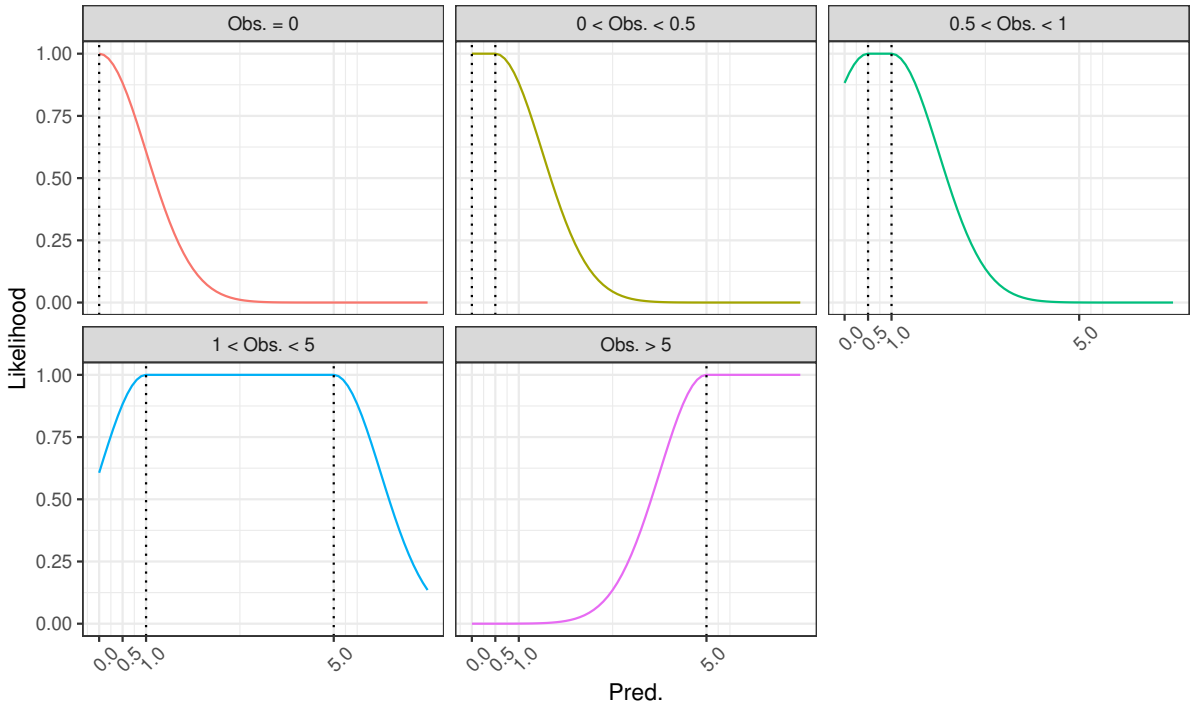

Figure 4: Gaussian Kernel likelihood function. This function accounts for the categorical nature of the observed data: any prediction that falls in the observed interval results in a maximal likelihood; when outside the observed interval, the likelihood decreases with the distance to the edge of the interval.

the coarser grid. For each larger grid cell, the upper bound of original bins was averaged over all of the smaller grid cells it encompassed. For the whole dataset and for each seasonal dataset separately, correlation was assessed using Spearmans's ρ, in order to identify monotonic but not necessarily linear relationships.

Rectangular regions were defined for yellowfin and albacore domains and were used to compare seasonal variations of larval CPUE, sampling effort and reference model outputs. To do this, the three variables were extracted in each region. Lower bound of larval sampling effort, and upper bound of larval CPUE, were averaged over each region. Model outputs were averaged over the same seasonal and regional aggregation. For each variable, averaged values were scaled to their maximal value to compare relative seasonal variations. Correlation between seasonal profiles of larval CPUE and model outputs were performed using Spearman's ρ.

5.2 Identical twin experiments

In order to assess the robustness of the newly defined cost functions, a set of experiments called identical twin experiments was conducted. A twin experiment consists in estimating parameters from a dataset constructed from model predictions. Since this pseudo-data is created with a priori known parameter values, the objective of the twin experiments is to evaluate how well the method finds these parameters when starting optimization from random parameter values, and when the data sampling mimics or not

the spatio-temporal coverage of the true observations. As such, the twin experiments can effectively assess the minimal data requirements for accurate parameter estimation, both in term of quantity and quality (categorical data, continuous data).

A single original solution (Table 2 and Supplementary Table 9) was used to generate seasonally aggregated spawning habitat index maps and larval density maps. After multiplication by the catchability parameter *q_sp_larvae*, these seasonal maps were then modified to create different experimental set-ups, in order to establish the data quality and quantity requirements:

- Data quality requirements:
  - Left as it is (i.e. continuous, cf Figure 5 and Supplementary Figure 20),
  - Classified into binned intervals (as in the Nishikawa dataset, cf Figure 6 and Supplementary Figure 21),
- Estimation of data quantity requirements: Random sampling of N grid cells,

where the number of observations N varies between the experiments. Additional twin experiments were performed, using pseudo-data with the same spatial coverage as the Nishikawa dataset (cf Supplementary Figures 26 and 27). All twin experiments presented here were performed using the Gaussian Kernel cost function, but all other cost functions were tested separately and validated as well.

Parameter	Min	Max	Value	Std. error
q_sp_larvae	0.0	100.0	0.0	0.004
a_sst_larvae	0.5	10.0	2.0	0.009
b_sst_larvae	25.5	35.0	31.0	0.015
alpha_hsp_prey	0.0	10.0	2.7	0.031
alpha_hsp_predator	0.0	10.0	1.8	0.064
beta_hsp_predator	0.0	10.0	2.3	0.022

Table 2: Spawning habitat parameter values and uncertainties. The range of values explored within the optimization process is also displayed. A twin experiment with continuous pseudo-data and full spatial coverage was used to evaluate the Hessian matrix at the point of minimum (i.e. original solution). Standard errors were computed as the square root of diagonal elements of the variance-covariance matrix, which was computed as the inverse of the Hessian matrix.

Besides, twin experiments configuration provides a perfect set-up to perform error and correlation analysis, which requires the evaluation of the Hessian matrix at the point of minimum. The correlations between parameter pairs need to be assessed and a list of independent parameters needs to be established prior to optimizing the likelihood function. Correlations were derived from the variance-covariance matrix being an inverse of the Hessian matrix evaluated in the vicinity of the function minimum, i.e. original parameter values in Table 2. For the pairs of correlated parameters with correlation $>$ 0.5, the parameter dependency is illustrated using the cost function 2D-profiles.

Note, in all twin experiments, only the parameters of spawning habitat index (Table 2) were estimated. So, when running the full population dynamics model, the parameters

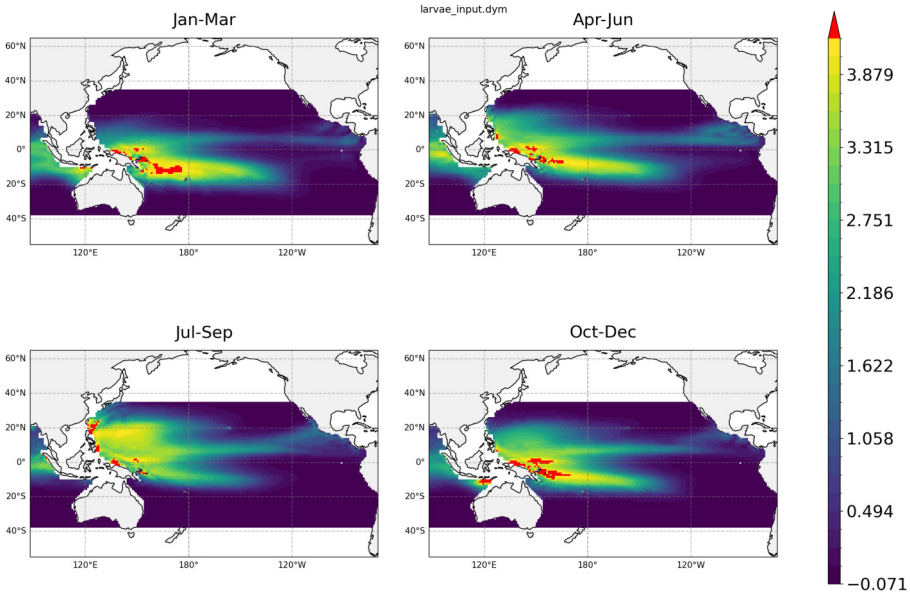

Figure 5: Larval density continuous output from the original solution, used as pseudo-data in twin experiments.

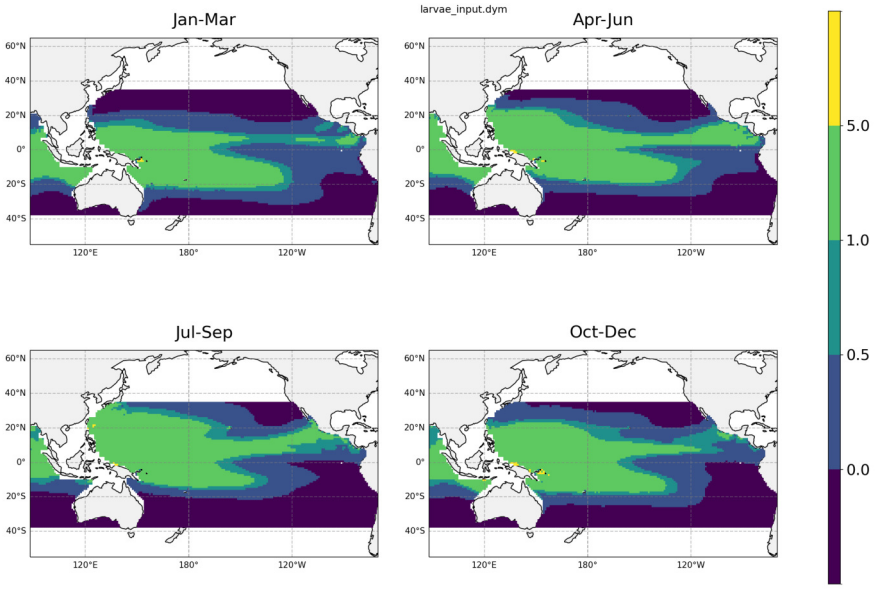

Figure 6: Larval density categorical output from the original solution, used as pseudo-data in twin experiments.

that govern the spatio-temporal distributions of mature adults were fixed at their values used in generating the pseudo-data.

For each twin experiment, 10 jitter runs with 10 different random combinations of starting parameter values were performed, to allow exploring the parameter space and to see if optimization converges to the known solution in all runs. Convergence to the original parameter values was assessed by measuring the difference between estimated and original value, standardized by the range in which the parameter values were explored (cf Min and Max bounds in Table 2).

Here, all experiments and the original solution were forced with the latest ERA5-NEMO-PISCES forcing dataset, with a monthly time resolution and 1 x 1° spatial resolution.

5.3 Parameter estimation using albacore gonad data

First, the spawning index generated as described in Section 3.2 was used in the simple SEAPODYM spawning habitat model, to estimate spawning habitat parameters and scaling factor *q_sp_larvae*. Second, it was used within the full population dynamics model to re-estimate spawning habitat parameters and two spawning season parameters (*spawning_season_start* and *spawning_season_peak*) in the current reference model of albacore tuna, which is forced with ERA-INTERIM-NEMO-PISCES model outputs. Since the changes (shifts, different duration and latitudinal extension of spawning migrations) in the spawning season may impact the modelled abundance of larvae, fisheries-specific catchability parameters were also re-estimated, fitting to fisheries (catch and length) data. The resulting model with re-estimated spawning season parameters was then compared to the reference model, and its outputs were analysed to assess if it resulted in a better fit to all data, including fisheries data and the gonad data-derived spawning index.

6 Results

6.1 Comparison of early life stage datasets to reference models

Before using early life stages datasets (described in Section 3) within SEAPODYM parameter estimation process, they were compared to the outputs of previous reference models of yellowfin (I. Senina, Hampton, et al. 2019) and albacore tuna (I. N. Senina et al. 2020).

6.1.1 Nishikawa larval CPUE versus yellowfin and albacore tuna reference models

Overall, categorical binned larval CPUE shows poor spatial correlation to continuous model outputs (Figures 7 and 9). Larval CPUE shows similar correlation to larval density

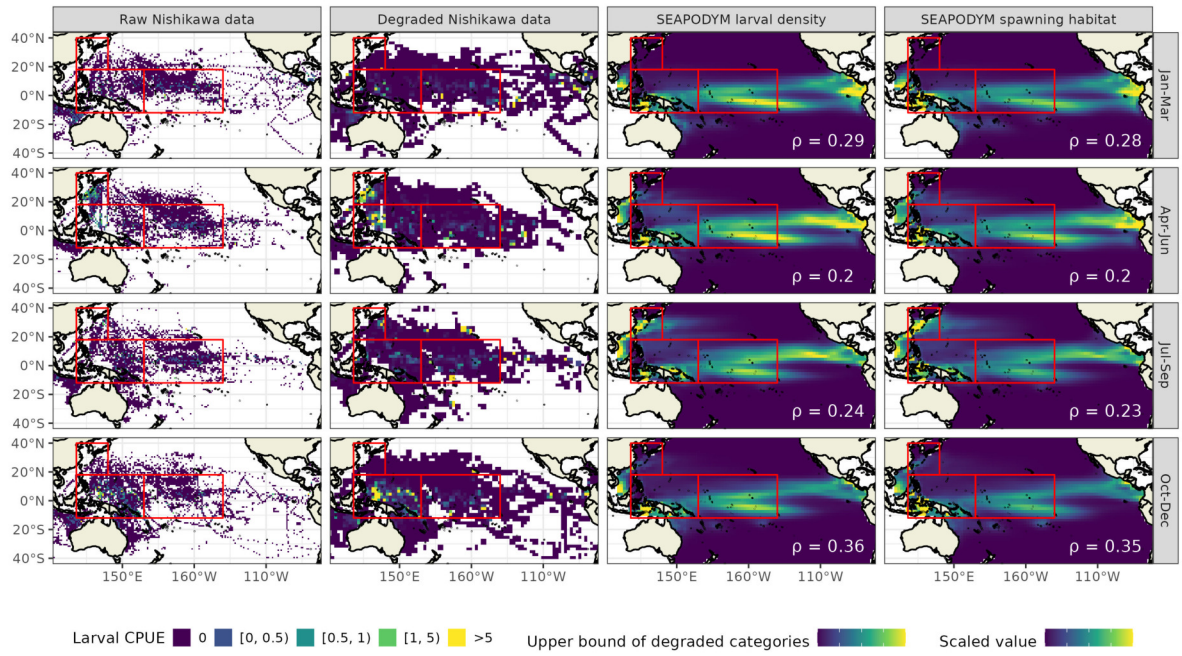

Figure 7: Comparison of yellowfin tuna Nishikawa larval CPUE and reference model outputs. Raw Nishikawa CPUE (1 x 1° grid) is displayed along degraded Nishikawa CPUE (2 x 2° grid) and reference model larval density and spawning habitat outputs. For each season, Spearman correlation was computed between degraded Nishikawa CPUE and reference model outputs. For plotting only, reference model outputs were scaled by their 99^{th} percentile value, all values greater than this percentile were down-scaled to 1.

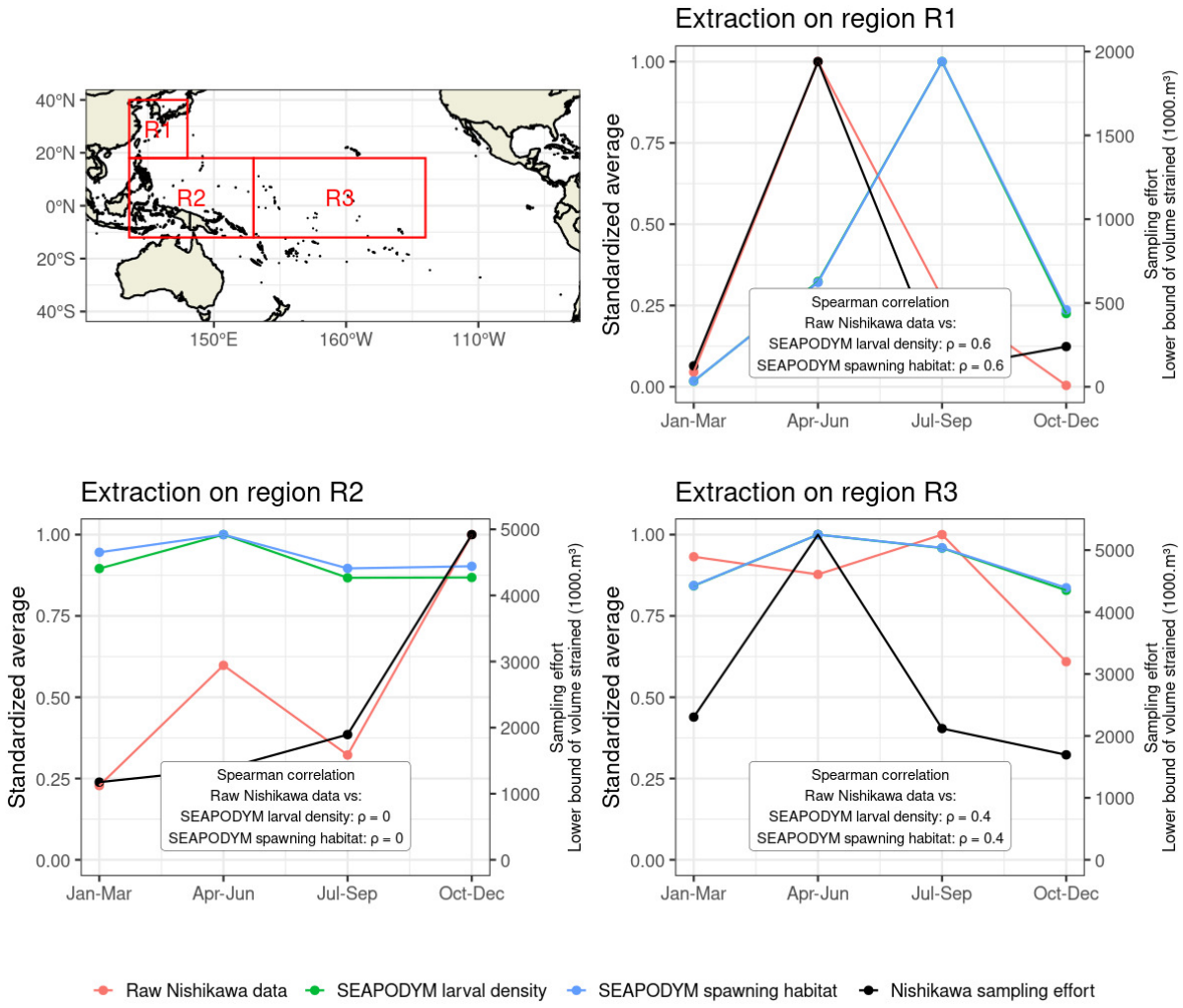

Figure 8: Seasonal variations of Nishikawa larval CPUE and reference model outputs for yellowfin tuna. Larval sampling effort, CPUE and reference model outputs were extracted in each region. Lower bound of larval sampling effort, and upper bound of larval CPUE, were averaged over each region. Model outputs were averaged over the same seasonal and regional aggregation. CPUE, model density and model habitat values were scaled to their respective maximal seasonal value to compare relative seasonal variations.

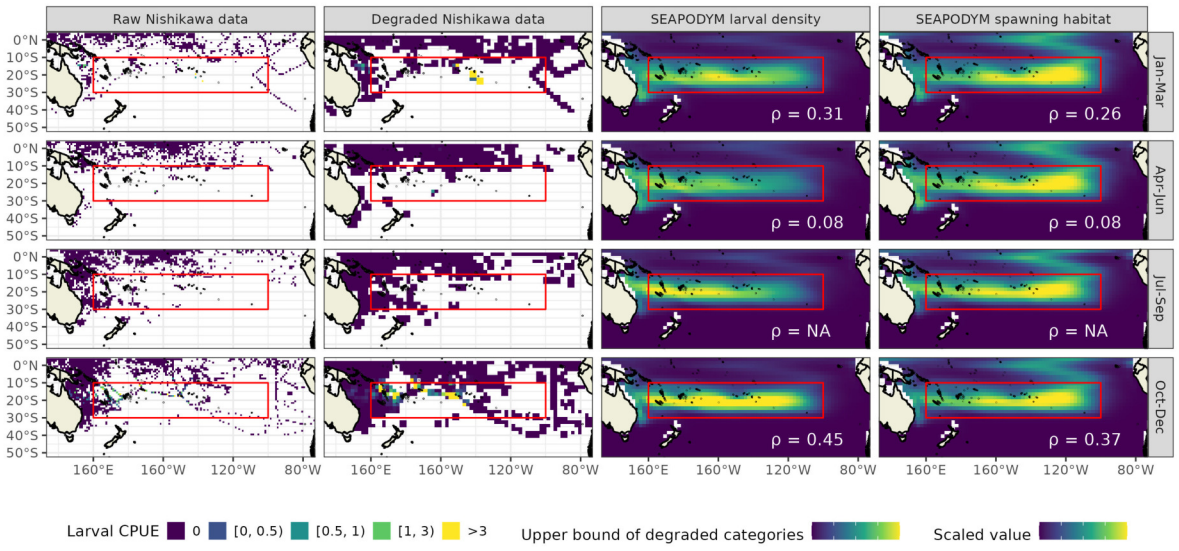

Figure 9: Comparison of albacore tuna Nishikawa larval CPUE and reference model outputs. Raw Nishikawa CPUE (1 x 1° grid) is displayed along degraded Nishikawa CPUE (2 x 2° grid) and reference model larval density and spawning habitat outputs. For each season, Spearman correlation was computed between degraded Nishikawa CPUE and reference model outputs. For plotting only, reference model outputs were scaled by their 99^{th} percentile value, all values greater than this percentile were down-scaled to 1.

(ρ= 0.28 and 0.29 for yellowfin and albacore resp.) and spawning habitat index (ρ= 0.27 and 0.23). Higher spatial correlation is observed during the Austral summer (Oct-December and Jan-Mar), especially for albacore tuna. For yellowfin tuna, sampling effort lacked coverage in the eastern Pacific, particularly on the coast of Central Americal, where the model predicted suitable habitat and high larvae densities.

For yellowfin tuna, seasonal variations of larval CPUE do not match neither model larval density nor larval habitat (Figure 8). Yet, sampling effort bias may have played a role in this mismatch (Supplementary Figure 22). In some regions, effort appears to be correlated to CPUE, suggesting it was concentrated on spawning grounds during the suspected, but not necessarily actual, spawning season. For instance, sampling effort might have driven larval CPUE up in April-June in region R1 and in October-December in region R2. In region R1, the low CPUE in July-September may have driven CPUE down and hidden some spawning still occuring. In region R2, effort was high and constant throughout all first three quarters, when CPUE variations somewhat matched predictions'. In the last quarter (October-December), we do not think the spike in effort to have driven CPUE up, as, at a smaller spatial scale, highest CPUE does no co-occur with highest volume strained (Supplementary Figure 22). In region R3, effort was high throughout the year, and even higher values in April-June did not drove CPUE up. Effort is thus unlikely to have biased CPUE seasonality in this region, and it is fair to assert that it does not match model predictions there.

For albacore tuna, seasonal variations of larval CPUE shows a close match to seasonal variations of model larval density (cf region R1 in Figure 10, where highest larval CPUE and modeled larval density were observed). While sampling effort was low in this region

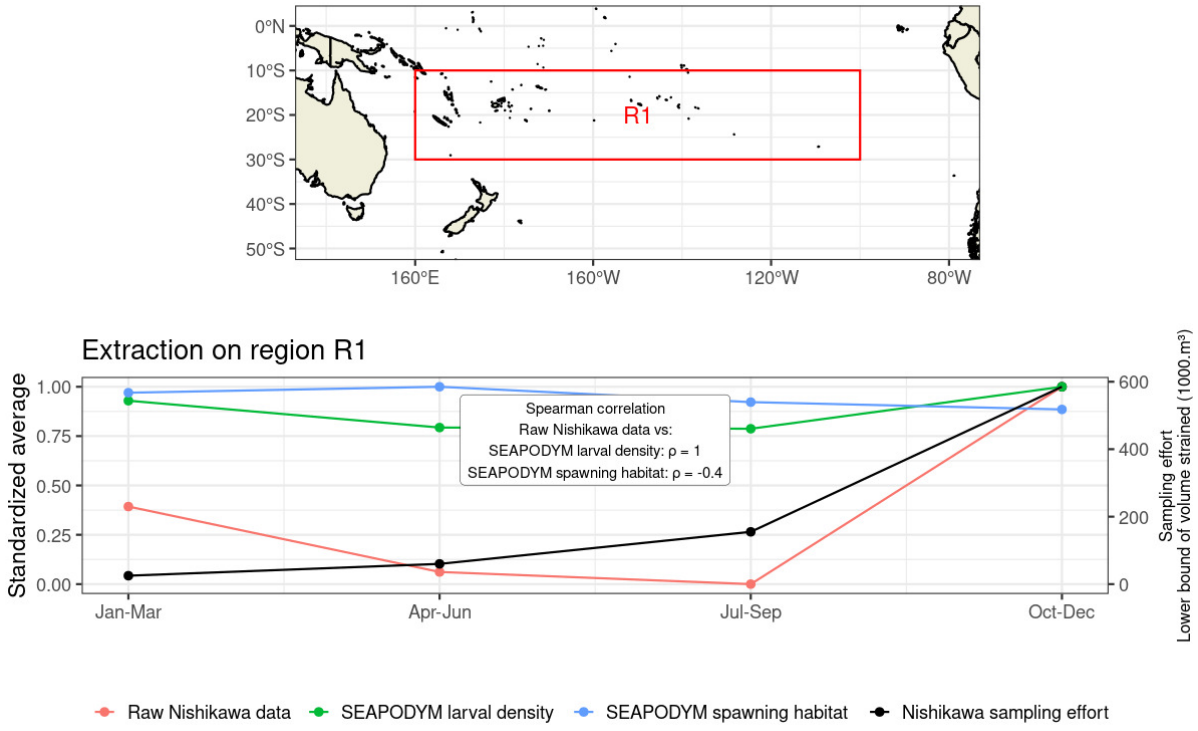

Figure 10: Seasonal variations of Nishikawa larval CPUE and reference model outputs for albacore tuna. Larval sampling effort, CPUE and reference model outputs were extracted in each region. Lower bound of larval sampling effort, and upper bound of larval CPUE, were averaged over each region. Model outputs were averaged over the same seasonal and regional aggregation. CPUE, model density and model habitat values were scaled to their respective maximal seasonal value to compare relative seasonal variations.

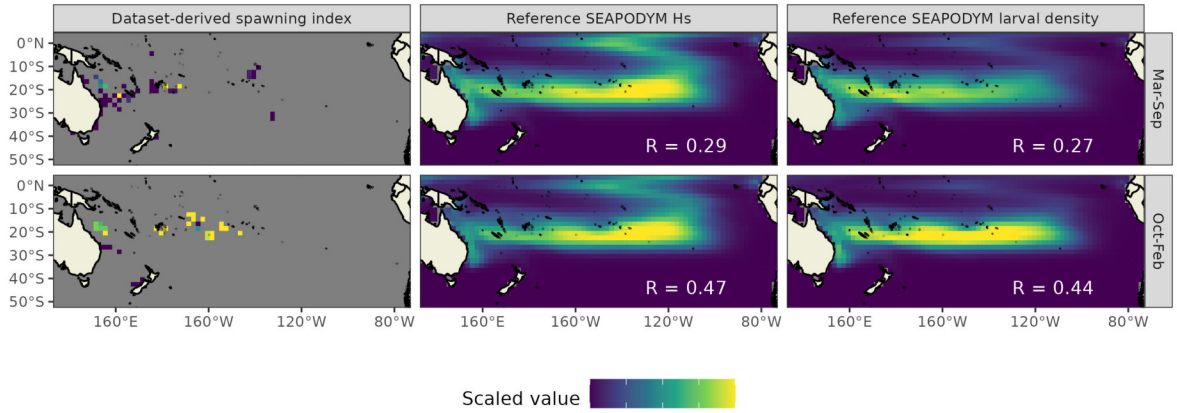

Figure 11: Comparison of spawning index to SEAPODYM reference albacore model outputs. For each season, Pearson correlation was computed between data-derived spawning index and aggregated reference model outputs. For plotting only, model outputs were scaled by their 99^{th} percentile value, all values greater than this percentile were down-scaled to 1.

during the first three quarters (see also Supplementary Figure 23), it is unlikely to be responsible for this match, as lowest effort in January-March did not prevent observing relatively high larval CPUE. Unlike model larval density, model spawning habitat do no show seasonal variations consistent with observed larval CPUE.

6.1.2 Gonad data-derived spawning index versus albacore tuna reference model

The spawning index derived from gonad data was used to evaluate the skill of previous reference SEAPODYM model predicting spawning season and larval habitat and distribution. Seasonal and spatial variations of observation-based spawning index were compared to SEAPODYM spawning habitat index and larval density.

Overall, Pearson correlation is greater with larval density (R=0.38) than with spawning habitat index (R=0.31), probably because larval density shows greater seasonal variations, and in accordance with the data-derived spawning index. Indeed, in region R1 where highest spawning index and modeled larval density are observed, seasonal variations of spawning index match those of model larval density but not those of spawning habitat index (Supplementary Figure 29).

However, within each season, spatial correlation is slighlty higher between gonad data-derived spawning index and SEAPODYM spawning habitat index (spawning season R=0.47 , outside spawning season R=0.29) than between spawning index and larval density (spawning season R=0.44 , outside spawning season R=0.27 ; Figure 11).

	q_sp_larvae	a_sst_larvae	b_sst_larvae	alpha_hsp_prey	alpha_hsp_predator	beta_hsp_predator
q_sp_larvae	1.00	0.22	0.24	0.13	**0.77**	**0.84**
a_sst_larvae		1.00	**0.98**	-0.06	-0.15	-0.14
b_sst_larvae			1.00	-0.13	-0.12	-0.12
alpha_hsp_prey				1.00	-0.20	-0.11
alpha_hsp_predator					1.00	**0.99**
beta_hsp_predator						1.00

Table 3: Parameter correlation matrix for the SEAPODYM habitat model fit to continuous data. Correlations were derived from the variance-covariance matrix being an inverse of the Hessian matrix evaluated in the vicinity of the function minimum, with continuous pseudo-data with full spatial coverage. Correlation coefficients greater than 0.5 are displayed in bold.

	q_sp_larvae	a_sst_larvae	b_sst_larvae	alpha_hsp_prey	alpha_hsp_predator	beta_hsp_predator
q_sp_larvae	1.00	0.27	0.28	0.06	**0.76**	**0.83**
a_sst_larvae		1.00	**0.98**	-0.06	-0.11	-0.10
b_sst_larvae			1.00	-0.14	-0.09	-0.09
alpha_hsp_prey				1.00	-0.26	-0.18
alpha_hsp_predator					1.00	**0.99**
beta_hsp_predator						1.00

Table 4: Parameter correlation matrix for the SEAPODYM habitat model fit to continuous data. Correlations were derived from the variance-covariance matrix being an inverse of the Hessian matrix evaluated in the vicinity of the function minimum, with continuous pseudo-data with full spatial coverage. Correlation coefficients greater than 0.5 are displayed in bold.

6.2 Parameter estimation using larval CPUE

6.2.1 Detection of correlated parameters

Fitting the pseudo-data to habitat and population dynamics model, it was found that some parameters of spawning habitat are highly correlated (Tables 3 and 4). In particular, there exist high correlations between parameters of the predator function, (*alpha_hsp_predator* and *beta_hsp_predator*; see Figures 12 and 13) even when using nearly ideal setting (full spatial coverage) with continuous data in the likelihood. Since function minimization works efficiently only with independent parameters, it is necessary to fix one parameter out of a pair of highly correlated parameters. In case the requirement of parameter independence is not fulfilled, the convergence of function minimization algorithm and its ability to estimate parameters are altered (see Supplementary Figure 25). Thus, *beta_hsp_predator*, was fixed and excluded from the estimation in the twin experiments.

6.2.2 Requirements for larval CPUE data

For the spawning habitat model, twin experiments showed that both continuous and categorical pseudo-datasets enabled parameter estimation (Figure 14). Convergence to original paramater values can be achieved with small amount of continuous observations (> 50 grid cells). A greater amount of categorical observations is necessary to reach convergence (> 200 grid cells), yet with lower accuracy, especially concerning the estimation of the optimal temperature (*b_sst_larvae*).

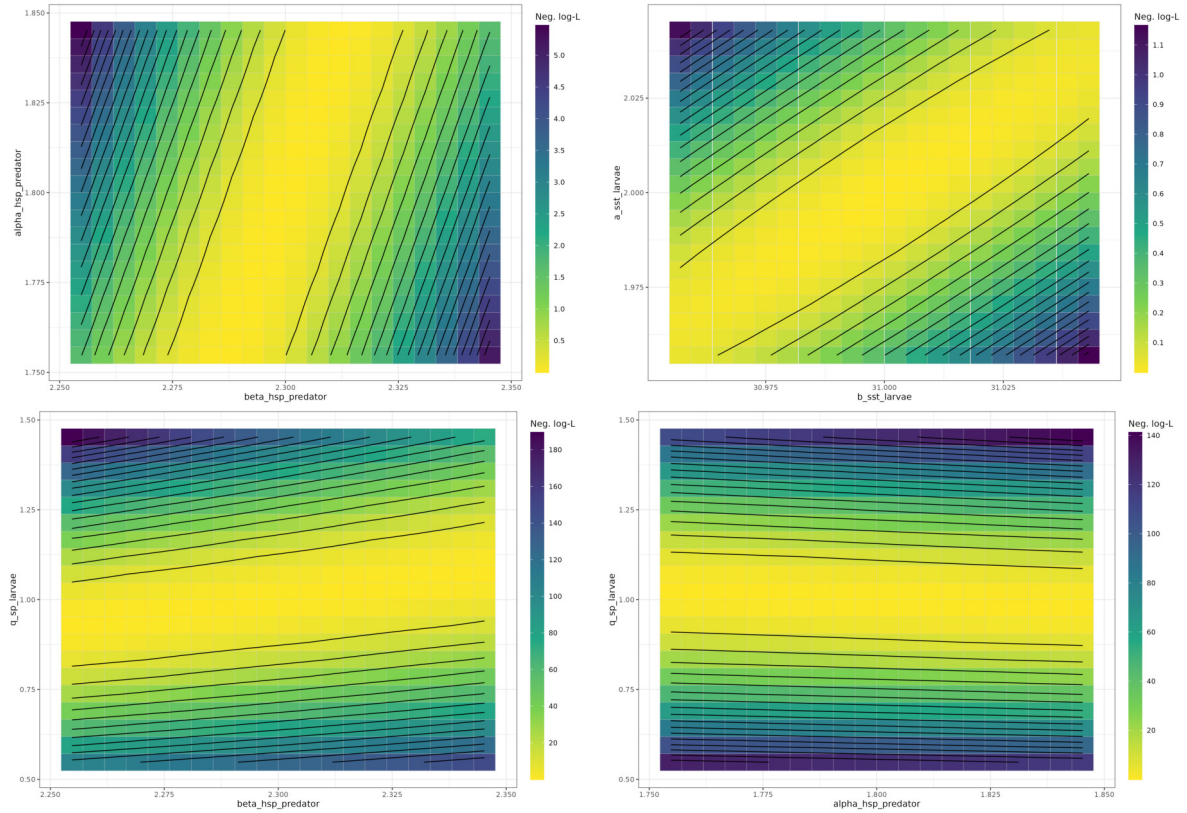

Figure 12: Cost function profiles for the SEAPODYM habitat model fit to continuous pseudo-data with full spatial coverage.

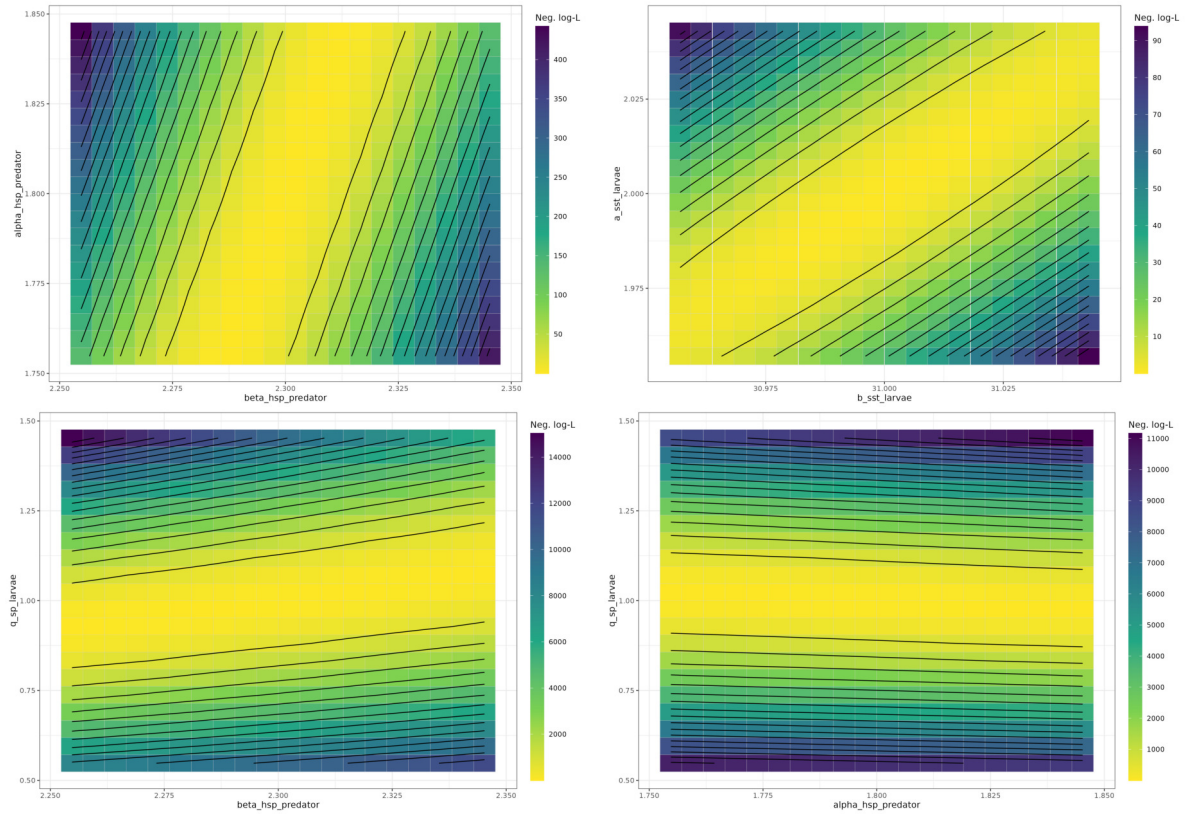

Figure 13: Cost function profiles for the SEAPODYM full population dynamics model fit to continuous pseudo-data with full spatial coverage.

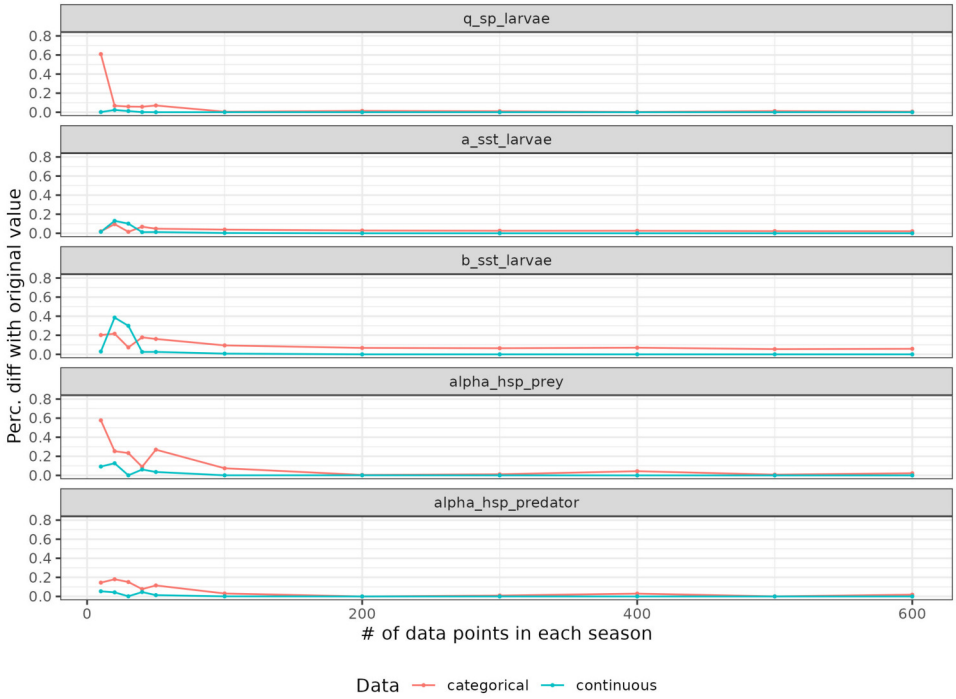

Figure 14: Outcome of twin experiments using the SEAPODYM habitat model. An original model with original parameter values was used to generate spawning habitat continuous or categorical outputs. Seasonal pseudo-datasets were extracted from these outputs, with varying quantities of randomly sampled grid cells. The ability of the optimization process to estimate parameter values accurately was estimated as the percentage difference to the original parameter values.

When informing parameters of the population dynamics model, very small amount (> 10 grid cells) of continuous observations enable estimation of the known parameter values with high accuracy (Figure 15). A greater amount of categorical observation is necessary to reach convergence, with relatively high residual error (>10%) for the estimation of *b_sst_larvae* and *alpha_hsp_prey* with 400 grid cells.

Twin experiments were also performed to assess if the spatial coverage of the non-zero observations in the Nishikawa dataset (grid cells with $N_{obs} > 0$) enabled accurate parameter estimation (see Supplementary Figures 26 and 27). These experiments showed that when using continuous pseudo-data, the spatial coverage of Nishikawa datasets is sufficient to allow accurate estimation of all habitat parameters (Table 5). When using categorical pseudo-data, this spatial coverage does not enable accurate estimation of habitat parameters. In particular, the prey function parameter is poorly estimated (*alpha_hsp_prey* parameter; Table 6).

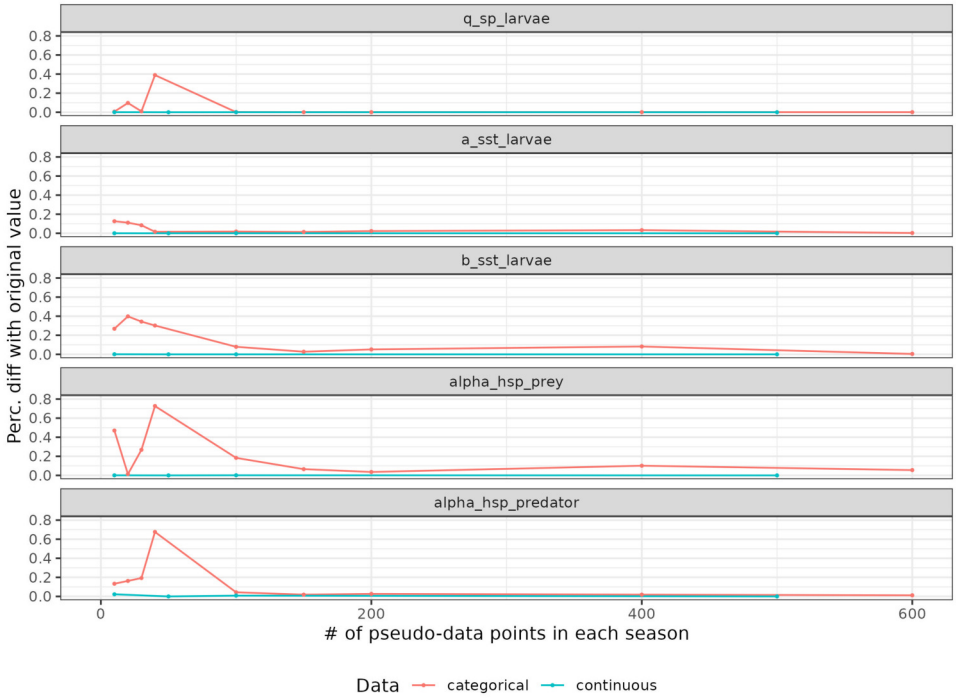

Figure 15: Outcome of twin experiments using the SEAPODYM full population dynamics model. An original model with original parameter values was used to generate larval density continuous or categorical outputs. Seasonal pseudo-datasets were extracted from these outputs, with varying quantities of randomly sampled grid cells. The ability of the optimization process to estimate parameter values accurately was estimated as the percentage difference to the original parameter values.

	Min	Max	Original value	Best twin experiment
a_sst_larvae	0.5	10.0	2.0	2.0
b_sst_larvae	25.5	35.0	31.0	31.0
alpha_hsp_prey	0.0	10.0	2.7	2.7
alpha_hsp_predator	0.0	10.0	1.8	1.8
beta_hsp_predator	0.0	10.0	2.3	2.3

Table 5: Estimated parameters for twin experiments using continuous pseudo-data with the same spatial coverage as the Nishikawa dataset. The pseudo-dataset used for optimization consisted in the larval density continuous outputs of an original model, subsampled over the same spatial coverage as the yellowfin tuna Nishikawa data (grid cells with $N_{obs} < 0$).

	Min	Max	Original value	Best twin experiment
a_sst_larvae	0.5	10.0	2.0	1.963
b_sst_larvae	25.5	35.0	31.0	30.870
alpha_hsp_prey	0.0	10.0	2.7	3.752
alpha_hsp_predator	0.0	10.0	1.8	1.743

Table 6: Estimated parameters for twin experiments using categorical pseudo-data with the same spatial coverage as the Nishikawa dataset. The pseudo-dataset used for optimization consisted in the larval density categorical outputs of an original model, subsampled over the same spatial coverage as the yellowfin tuna Nishikawa data (grid cells with $N_{obs} < 0$).

6.3 Parameter estimation using albacore gonad data

6.3.1 Habitat model

Fitting the SEAPODYM spawning habitat model to the seasonal spawning index derived from the albacore gonad data (cf 3.2) resulted in different thermal preference and functional response to primary production as a proxy of the larval prey (Table 7), compared to the reference model.

	Min	Max	Reference model	Re-fitted model
a_sst_larvae	0.5	2.0	2.00000	2.00000
b_sst_larvae	23.5	26.5	23.50000	24.99000
alpha_hsp_prey	0.00025	0.004	0.00025	0.00025
alpha_hsp_predator	1.0	2.4	1.00100	2.40000
beta_hsp_predator	1.5	3.0	2.17800	2.34900
q_sp_larvae	0.0	100.0	NA	0.94760

Table 7: Comparison of spawning habitat parameters of the reference and re-fitted SEAPODYM spawning habitat model. The re-fitted habitat model used albacore gonad data-derived spawning index to re-estimate spawning habitat parameters.

Re-fitted habitat model has higher spatial correlation to the gonad data-derived data (R=0.47 vs. 0.31), due to a better spatial correlation during spawning season (R=0.7 vs. 0.47 ; Figure 16). However, the habitat index itself does not explain the seasonal variability in the data (R=0.28 outside spawning season, and see Supplementary Figure 30). Indeed, the modelled spawning habitat index, located mainly within the tropical zone is not expected to have marked seasonal variability (see the seasonal SST, prey and predator density in Figure Supplementary 28).

The seasonal variability in spawning status is thus driven by seasonal variations of adult density.

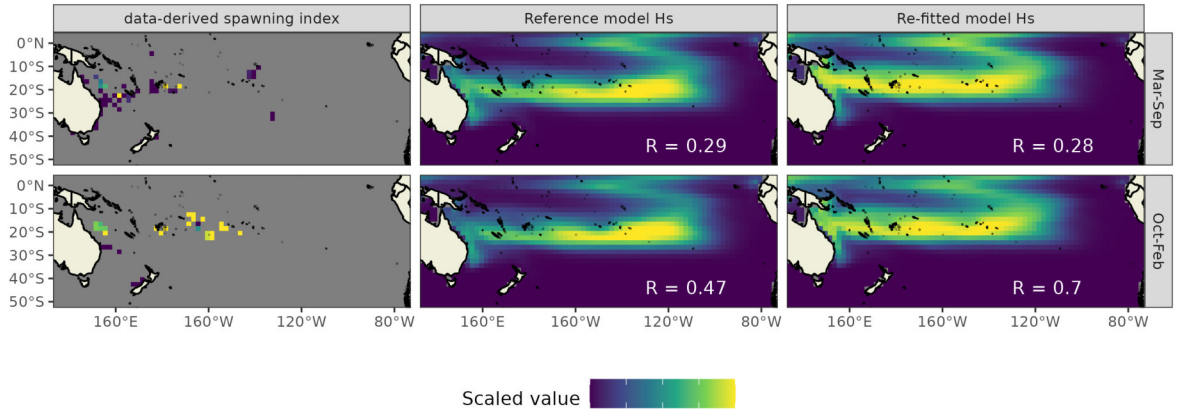

Figure 16: Albacore gonad data-derived spawning index versus reference and re-fitted SEAPODYM habitat model outputs. For each season, Pearson correlation was computed between data-derived spawning index and aggregated model spawning habitat. For plotting only, model outputs were scaled by their 99^{th} percentile value, all values greater than this percentile were down-scaled to 1.

6.3.2 Population dynamics model

To explain the observed seasonal variability of spawning index, we re-estimated both spawning habitat parmaters and spawning season parameters that drive the seasonal migrations of adult albacore in our population dynamics model (*spawning_season_start* and *spawning_season_peak*). Hence the reference model outputs were fitted to the gonad data-derived spawning index in the attempt to improve these parameters. The scaling parameter *q_sp_larvae* was simultaneously estimated.

Since the spawning success and hence the larval abundance, depends on adult density in the spawning site, which in turn depends on the seasonal migration and spawning habitat parameters, changes of these parameters lead to changes of the model state variable. Hence, additional estimation of fisheries parameters was undertaken by optimizing the catch and length likelihoods.

This process resulted in the 23 days delay of the spawning season peak, and a day-length dependent season start modified from 1.05 to 1.09 (Table 8), which corresponds to a minimal latitude of 16.5° for the migration to occur.

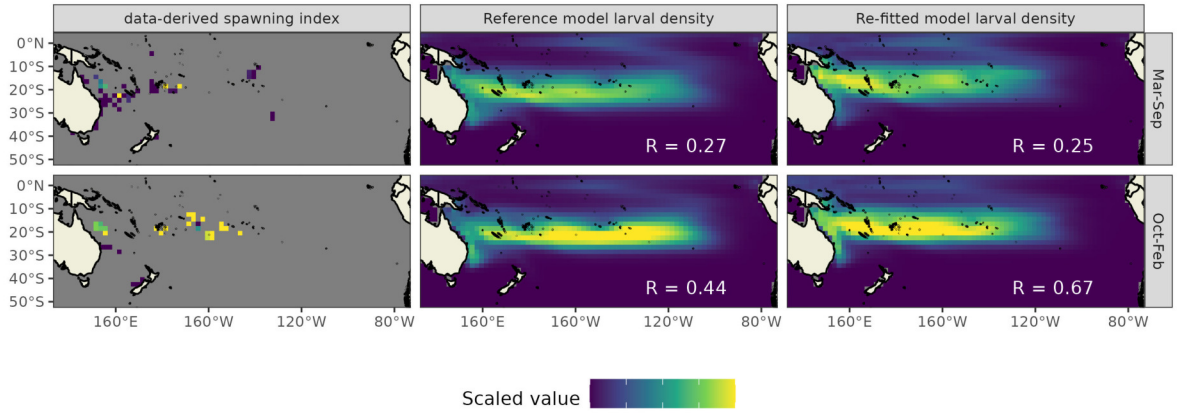

Figure 17: Albacore gonad data-derived spawning index versus reference and re-fitted SEAPODYM full population dynamics model outputs. For each season, Pearson correlation was computed between data-derived spawning index and aggregated model larval density. For plotting only, model outputs were scaled by their 99^{th} percentile value, all values greater than this percentile were down-scaled to 1.

	Min	Max	Reference model	Re-fitted model
a_sst_larvae	0.5	2.0	2	2
b_sst_larvae	23.5	26.5	23.5	25.06
alpha_hsp_prey	0.00025	0.004	0.00025	0.0002501
alpha_hsp_predator	1.0	2.4	1.001	2.381
beta_hsp_predator	1.5	3.0	2.178	2.296
spawning_season_peak	105	190	117.1	140
spawning_season_start	0.95	1.2	1.054	1.094
q_sp_larvae	0.0	100.0	NA	0.7992

Table 8: Comparison of spawning habitat and spawning season parameters of the reference and re-fitted SEAPODYM population dynamics model. The re-fitted model used albacore gonad data-derived spawning index to re-estimate spawning habitat and spawning season parameters.

The parameter re-estimation improved the correlation to spawning index, with R=0.58 (vs. R=0.38 for the reference model) for both seasons. It mostly improved correlation during the spawning season (R=0.67 vs. 0.44), while it did not improve correlation outside spawning season (R=0.25 vs. 0.27).

Compared to the reference model, a slightly better match with the data was obtained for the seasonal variations of larval density (cf region R1 in Supplementary Figures 29 and 30). Re-estimation of fisheries parameters allowed a similar fit to catch data as in the reference model, with a slightly worse correlation and normalized mean square error and a slightly better variance ratio (Figure 18).

(a) Reference model (b) Re-fitted model

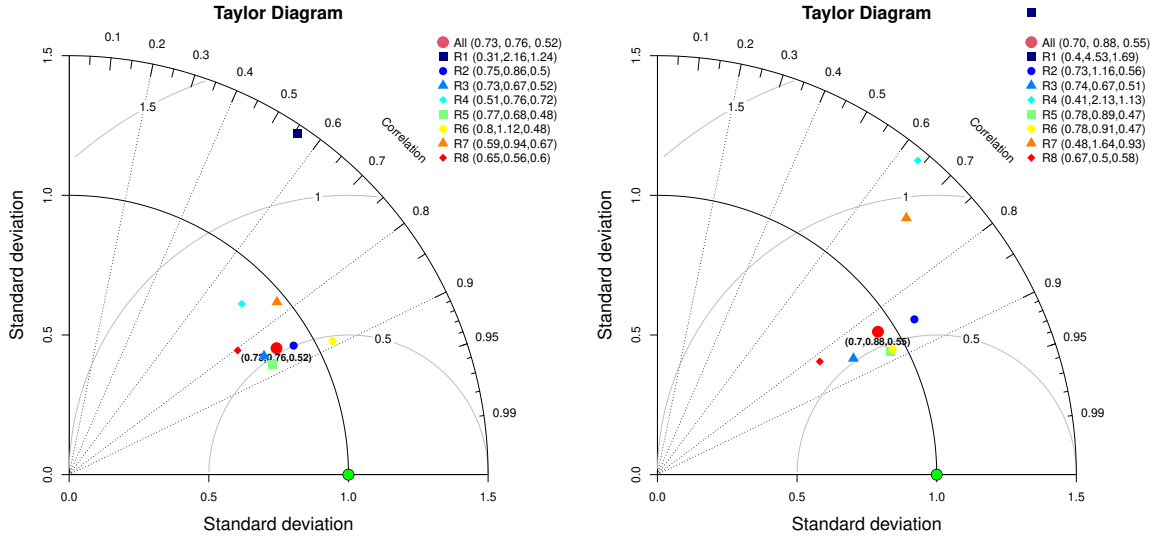

Figure 18: Comparison of fit to catch data in the reference and re-fitted model. Taylor diagrams represent the fit of predicted to observed catch: Pearson's R, variance ratio and Normalized Root Mean Square Error. All 3 metrics were computed for the whole training dataset and for different rectangular regions (not displayed here, used in the MFCL stock-assessment model).

7 Discussion

The new implementations in the SEAPODYM model enable integration of new types of data to inform the modelling of tuna early life stages dynamics and improve reference models. While the methodology is established and validated, uncertainty remains regarding the availability of data to successfully inform the reference model parameters. In particular, it was shown that with the categorical data, optimal spawning habitat parameters could not be re-estimated, irrespective of data quantity. Hence the categorical nature of the Nishikawa larval CPUE data is a limiting factor for its use in the parameter estimation. Moreover, it is likely that even if the access to the original continuous data can be granted, some models, e.g., for bigeye tuna, will not benefit from the use of this dataset given the data scarcity and known issues with species identification from larval samples.

Geo-referenced spawning status samples of South Pacific albacore tuna, however, proved to be suitable and adequate for estimating the spawning season parameters, validating the timing and the extent that were previously estimated using fisheries data.

Parameter estimation with larval data in the likelihood showed that some parameters of the SEAPODYM's spawning habitat model are highly correlated, even in the case of perfect "data" (derived from model outputs) and full spatial coverage. These results helped configure well-posed optimization problems in this work, estimating only independent parameters. The parameter correlation analysis will also be useful for future work on updating the reference models.

In particular, this work highlighted potential issues associated with the uniqueness of solutions in twin experiments. Indeed, even with large amounts of continuous pseudo-data, twin experiments did not always converge to the original solutions depending on the starting point. Hence, selecting only the best jitter run could impact the results of our analysis and lead to underestimation of data quantity needed to accurately estimate parameters and overestimation of robustness of the method. This problem will be addressed in the future work.

In this work we studied how the model performs with ideal data, thus removing uncertainty linked to the environment forcing and to model ability to describe the data. The use of larval CPUE data in the real setting is certainly a more complex and challenging task. On the other hand, we used the larval data alone, without combining it with fisheries and tagging data in the likelihood. Further work will focus on parameter estimation in the full likelihood context, to see if adding the early life stages data in the full likelihood will allow an improvement of observability and hence unbiased estimation of spawning parameters.

While raw categorical larval CPUE may prove inappropriate for parameter estimation, another options could be to use continuous outputs of geostatistical models trained on larval presence/absence from this dataset (Ijima and Jusup 2023) as an intermediate processing step of the observational dataset. The benefit of using such data is not only the continuity, but also the greater spatial coverage, which facilitates parameter estimation.

8 Acknowledgements

We would like to thank Dr. Jessica Farley from the Commonwealth Scientific and Industrial Reaserch Organisation (CSIRO) for providing the South Pacific albacore female gonad histological dataset.

References

Richards, W. J. and T. Potthoff (1974). "Analysis of the Taxonomic Characters of Young Scombrid Fishes, Genus Thunnus". en. In: *The Early Life History of Fish*. Ed. by John H. S. Blaxter. Berlin, Heidelberg: Springer, pp. 623–648. ISBN: 978-3-642-65852-5. DOI: 10.1007/978-3-642-65852-5_50.

Nishikawa, Yasuo et al. (1985). "Average Distribution of Larvae of Oceanic Species of Scombroid Fishes, 1956—1981." en. In: *Far Seas Fisheries Research Laboratory*.

Farley, Jessica H., Ashley J. Williams, et al. (Apr. 2013). "Reproductive Dynamics and Potential Annual Fecundity of South Pacific Albacore Tuna (Thunnus alalunga)". en. In: *PLOS ONE* 8.4. Publisher: Public Library of Science, e60577. ISSN: 1932-6203. DOI: 10.1371/journal.pone.0060577. URL: https://journals.plos.org/plosone/article?id=10.1371/journal.pone.0060577 (visited on 02/26/2024).

Farley, Jessica H., Simon D. Hoyle, et al. (Jan. 2014). "Maturity Ogives for South Pacific Albacore Tuna (Thunnus alalunga) That Account for Spatial and Seasonal Variation in the Distributions of Mature and Immature Fish". en. In: *PLOS ONE* 9.1. Publisher: Public Library of Science, e83017. ISSN: 1932-6203. DOI: 10.1371/journal.pone.0083017. URL: https://journals.plos.org/plosone/article?id=10.1371/journal.pone.0083017 (visited on 02/21/2024).

Senina, Inna, John Hampton, et al. (2019). *Spatial structure and regional connectivity of bigeye and yellowfin tuna stocks in the WCPO derived from the reference SEAPODYM models — WCPFC Meetings*. Information Paper. 19th Regular Session of the Scientific Committee. URL: https://meetings.wcpfc.int/node/19371 (visited on 07/16/2024).

Senina, Inna, Patrick Lehodey, et al. (Mar. 2020). "Integrating tagging and fisheries data into a spatial population dynamics model to improve its predictive skills". In: *Canadian Journal of Fisheries and Aquatic Sciences* 77.3. Publisher: NRC Research Press, pp. 576–593. ISSN: 0706-652X. DOI: 10.1139/cjfas-2018-0470. URL: https://cdnsciencepub.com/doi/full/10.1139/cjfas-2018-0470 (visited on 07/05/2023).

Senina, Inna N. et al. (May 2020). "Quantitative modelling of the spatial dynamics of South Pacific and Atlantic albacore tuna populations". en. In: *Deep Sea Research Part II: Topical Studies in Oceanography*. Oceanic biodiversity under climate change: shifts in natural and human systems 175, p. 104667. ISSN: 0967-0645. DOI: 10.1016/j.dsr2.2019.104667. URL: https://www.sciencedirect.com/science/article/pii/S0967064519301511 (visited on 07/05/2023).

Buenafe, Kristine Camille V. et al. (July 2022). "A global, historical database of tuna, billfish, and saury larval distributions". en. In: *Scientific Data* 9.1, p. 423. ISSN: 2052-4463. DOI: 10.1038/s41597-022-01528-7. URL: https://www.nature.com/articles/s41597-022-01528-7 (visited on 08/16/2023).

Williams, Graham et al. (Mar. 2022). *rattle: Graphical User Interface for Data Science in R*. URL: https://cran.r-project.org/web/packages/rattle/index.html (visited on 04/26/2024).

Ijima, Hirotaka and Marko Jusup (Apr. 2023). *Tuna and billfish larval distributions in a warming ocean*. en. arXiv:2304.09442 [physics, q-bio]. URL: http://arxiv.org/abs/2304.09442 (visited on 05/21/2023).

Therneau, Terry et al. (Dec. 2023). *rpart: Recursive Partitioning and Regression Trees*. URL: https://cran.r-project.org/web/packages/rpart/index.html (visited on 04/26/2024).

9 Supplementary Material

9.1 Cost functions based on different likelihood functions

Categorical equivalent of a Poisson Likelihood

$$-lnL(\theta|X_{obs}) = \begin{cases} -w_0 \cdot \log(\frac{X_{pred}}{2\sigma}) & \text{if } X_{obs} = 0 \\ -\log(\int_{X_{obs1}}^{X_{obs2}} \frac{{X_{pred}}^x e^{-X_{pred}}}{\Gamma(x+1)}\, dx) & \text{if } X_{obs} > 0 \end{cases} \tag{8}$$

where w_0 is the weighting factor for null observations.

Categorical equivalent of a Zero-Inflated Poisson Likelihood

$$-lnL(\theta|X_{obs}) = \begin{cases} -w_0 \cdot \log(p * (1-p) \cdot e^{-X_{pred}}) & \text{if } X_{obs} = 0 \\ -\log(\int_{X_{obs1}}^{X_{obs2}} \frac{X_{pred}^x e^{-X_{pred}}}{\Gamma(x+1)}\, dx) & \text{if } X_{obs} > 0 \end{cases} \tag{9}$$

Categorical equivalent of a Zero-Inflated Negative Binomial Likelihood

$$-lnL(\theta|X_{obs}) = \begin{cases} -w_0 \cdot \log\left(p + (1-p)\left(\frac{\beta}{1+\beta}\right)^{\beta \frac{X_{\text{pred}}}{1-p}}\right) & \text{if } X_{\text{obs}} = 0 \\ -\log\left(\int_{X_{obs1}}^{X_{obs2}} \frac{X_{\text{pred}}^x e^{-X_{\text{pred}}}}{\Gamma(x+1)}\, dx\right) & \text{if } X_{\text{obs}} > 0 \end{cases} \tag{10}$$

Categorical equivalent of a Truncated Poisson Likelihood

$$-lnL(\theta|X_{obs}) = -\log(L(\theta|X_{obs})) = \begin{cases} -w_0 \cdot \log\left(\frac{e^{-X_{pred}}}{1-e^{-X_{pred}}}\right) & \text{if } X_{obs} = 0 \\ -\log(\int_{X_{obs1}}^{X_{obs2}} \frac{{X_{pred}}^x e^{-X_{pred}}}{\Gamma(x+1)}\, dx) & \text{if } X_{obs} > 0 \end{cases} \tag{11}$$

9.2 Spawning habitat index

The spawning habitat index Hs is defined as a function of surface temperature (SST), larvae prey density (Λ; proportional to primary productivity) and larvae predator density (F_1):

$$H_s = f_1(SST; T^*, \sigma) \cdot f_2(\Lambda; \alpha) \cdot f_3(F_1; \alpha_F, \beta_F), \tag{12}$$

These three functions are defined between 0 and 1 as follows. The thermal conditions are described by

$$f_1 = e^{-\frac{(SST-T^*)^2}{2\sigma^2}}, \tag{13}$$

a Gaussian function with two parameters T^* and σ, being the optimal temperature and thermal tolerance interval of larvae. The function f_2 is the analogue of the Holling type III functional response function with n=2:

$$f_2 = \frac{\Lambda^n}{\alpha + \Lambda^n}, \tag{14}$$

with αthe inverse of searching efficiency and Λthe prey density. The third function f_3 is the log-normal distribution function rescaled to (0, 1) allowing selection of the optimal window of micronekton densities F1 in the surface layer:

$$f_3 = \frac{1}{F_1 \cdot e^{0.5\beta_F^2 - \alpha_F}} \cdot e^{-\frac{(\log(F_1) - \alpha_F)^2}{2\beta_F^2}}, \tag{15}$$

with parameters α_F and β_F are the mean and standard deviation of log-normal distribution function, and F_1 is the surface micronekton densities.

9.3 Figures and tables

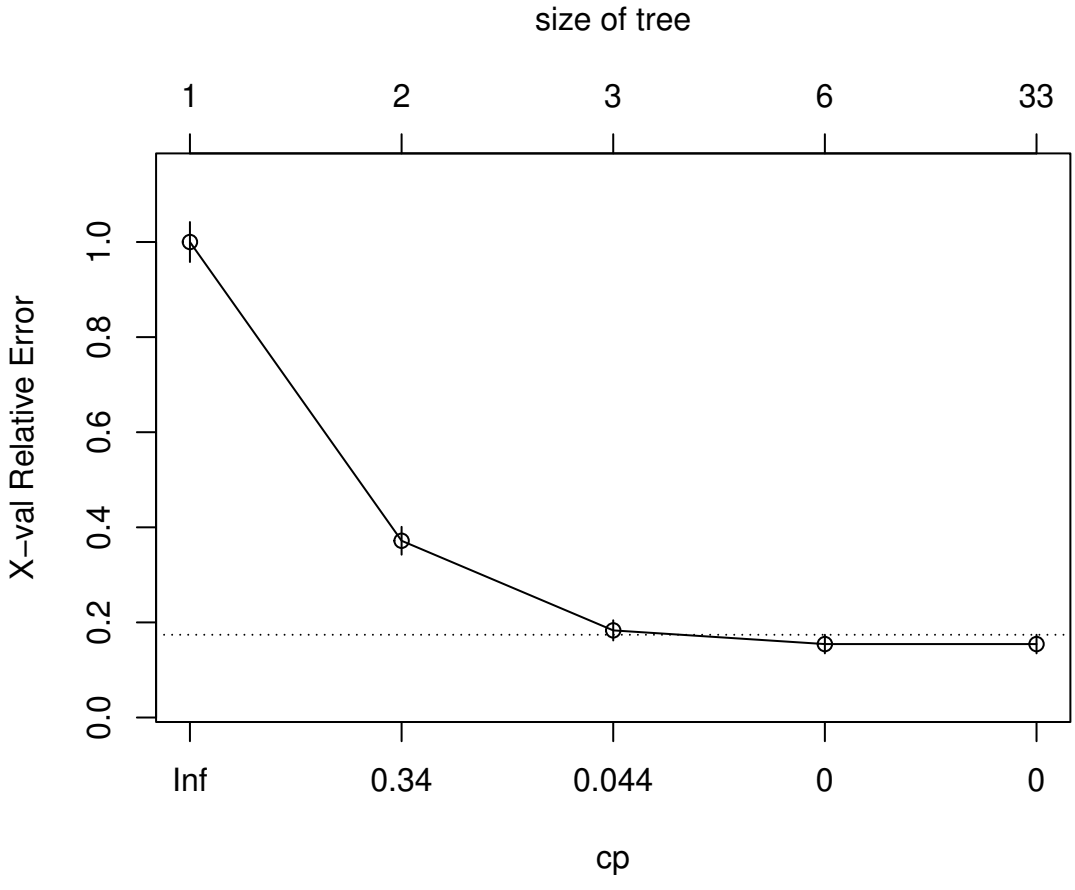

Figure 19: Hierarchical clustering of spawning status samples - Optimal tree complexity computed from 10-fold cross-validation. Graph generated using the *rpart* R package (Therneau et al. 2023).

Table 9: Parameter values from the original solution used for twin experiments.

Parameter	Min	Max	Value
q_sp_larvae	0.0	100.0	0.05
a_sst_larvae	0.5	10.0	2
b_sst_larvae	25.5	35.0	31
alpha_hsp_prey	0.0	10.0	2.7
alpha_hsp_predator	0.0	10.0	1.8
beta_hsp_predator	0.0	10.0	2.3
likelihood_larvae_sigma	0.0	10.0	1
likelihood_larvae_beta	0.0	1.0	0.5
likelihood_larvae_probzero	0.0	1.0	0.5
a_sst_spawning	1.0	2.5	1.2
b_sst_spawning	29.0	36.0	33
nb_recruitment	0.05	0.95	0.09
a_adults_spawning	0.01	2	10
hp_cannibalism	0	20	1
spawning_season_peak	0	365	128.37
spawning_season_start	0.95	1.4	1.4
a_sst_habitat	1.5	10.5	1.6
b_sst_habitat	0.0	27.0	15
T_age_size_slope	1.0	3.0	2.5
thermal_func_delta1	0.0	0.05	0.02
thermal_func_delta2	0.0	0.25	0
thermal_func_delta3	0.0	10.0	3.25
a_oxy_habitat	0.0001	0.125	0
b_oxy_habitat	0.0	3.0	0.41
eF_habitat_epi	0.35	1.0	0.45
eF_habitat_meso	0.35	1.0	0.45
eF_habitat_mmeso	0.35	1.0	0.45
eF_habitat_bathy	0.0	10.0	0
eF_habitat_mbathy	0.0	10.0	0
eF_habitat_hmbathy	0.35	1.0	0.55
sigma_species	0	0.06	0.9
c_diff_fish	0	1.0	0.3
MSS_species	0.7	1.0	0.8
MSS_size_slope	0.85	1.1	1
Mp_mean_max	0.0	0.15	0.1
Mp_mean_exp	0.01	0.25	0.15
Ms_mean_max	0.0	0.006	0
Ms_mean_slope	0.5	1.35	1.1
M_mean_range	0.05	3.5	2
q_sp_fishery_L1	0.0	0.1	0.01
q_sp_fishery_L2	0.0	0.1	0

Continued on next page

Table 9 – continued from previous page

Parameter	Min	Max	Value
q_sp_fishery_L3	0.0	0.1	0.01
q_sp_fishery_L4	0.0	0.1	0
q_sp_fishery_L5	0.0	0.1	0.01
q_sp_fishery_L6	0.0	0.1	0.01
q_sp_fishery_L7	0.0	0.1	0.01
q_sp_fishery_L8	0.0	0.1	0
q_sp_fishery_S9	0.0	0.02	0
q_sp_fishery_S10	0.0	0.01	0.01
q_sp_fishery_S11	0.0	0.1	0
q_sp_fishery_S12	0.0	0.1	0.02
q_sp_fishery_S13	0.0	0.1	0.02
q_sp_fishery_S14	0.0	0.1	0.01
q_sp_fishery_S15	0.0	0.1	0.02
q_sp_fishery_P16	0.0	0.01	0
q_sp_fishery_O17	0.0	0.05	0
s_sp_fishery_L1	0.05	0.5	0.1
s_sp_fishery_L2	10	30	28.57
s_sp_fishery_L3	5	40	19.6
s_sp_fishery_L4	10	30	16.32
s_sp_fishery_L5	0.05	40	33.2
s_sp_fishery_L6	0	35	17.67
s_sp_fishery_L7	1.5	35	14.91
s_sp_fishery_L8	0.1	35	15.63
s_sp_fishery_S9	1.5	25	24.88
s_sp_fishery_S10	0.05	25	8.57
s_sp_fishery_S11	1.5	25	7.8
s_sp_fishery_S12	1.5	35	10.58
s_sp_fishery_S13	0.05	55	0.05
s_sp_fishery_S14	5	55	5.17
s_sp_fishery_S15	5	55	9.97
s_sp_fishery_P16	0.05	25	14
s_sp_fishery_O17	1.05	24	30

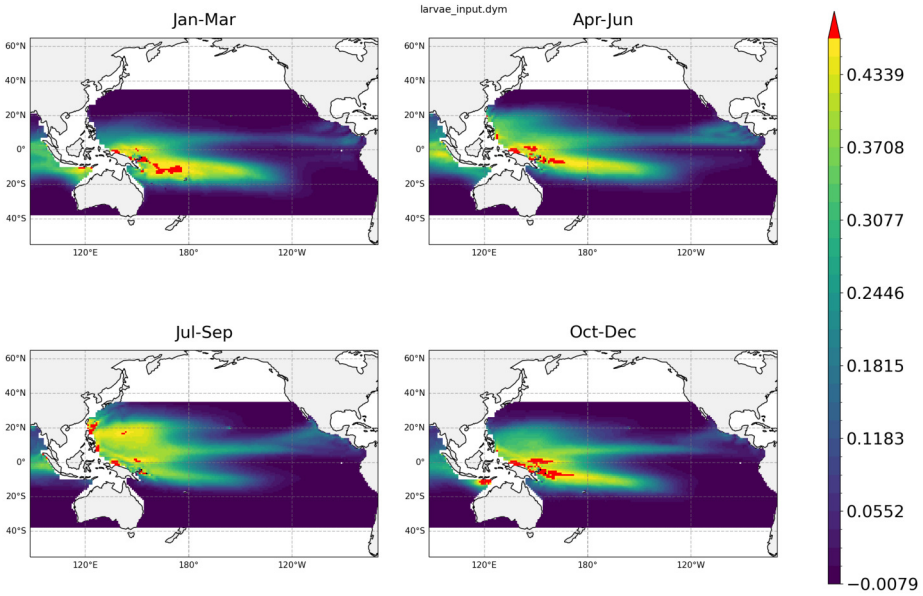

Figure 20: Spawning habitat index output from the original solution used for twin experiments.

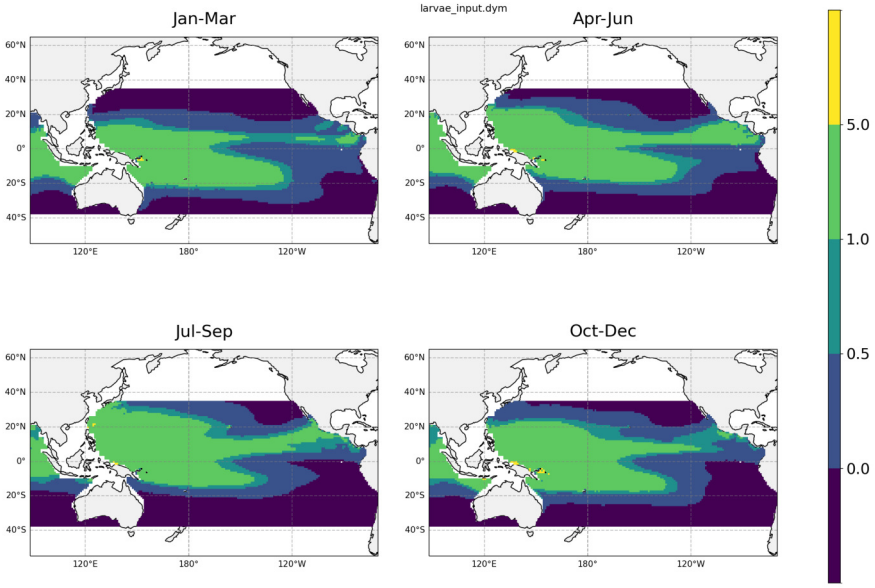

Figure 21: Larval density categorical output from the original solution used for twin experiments.

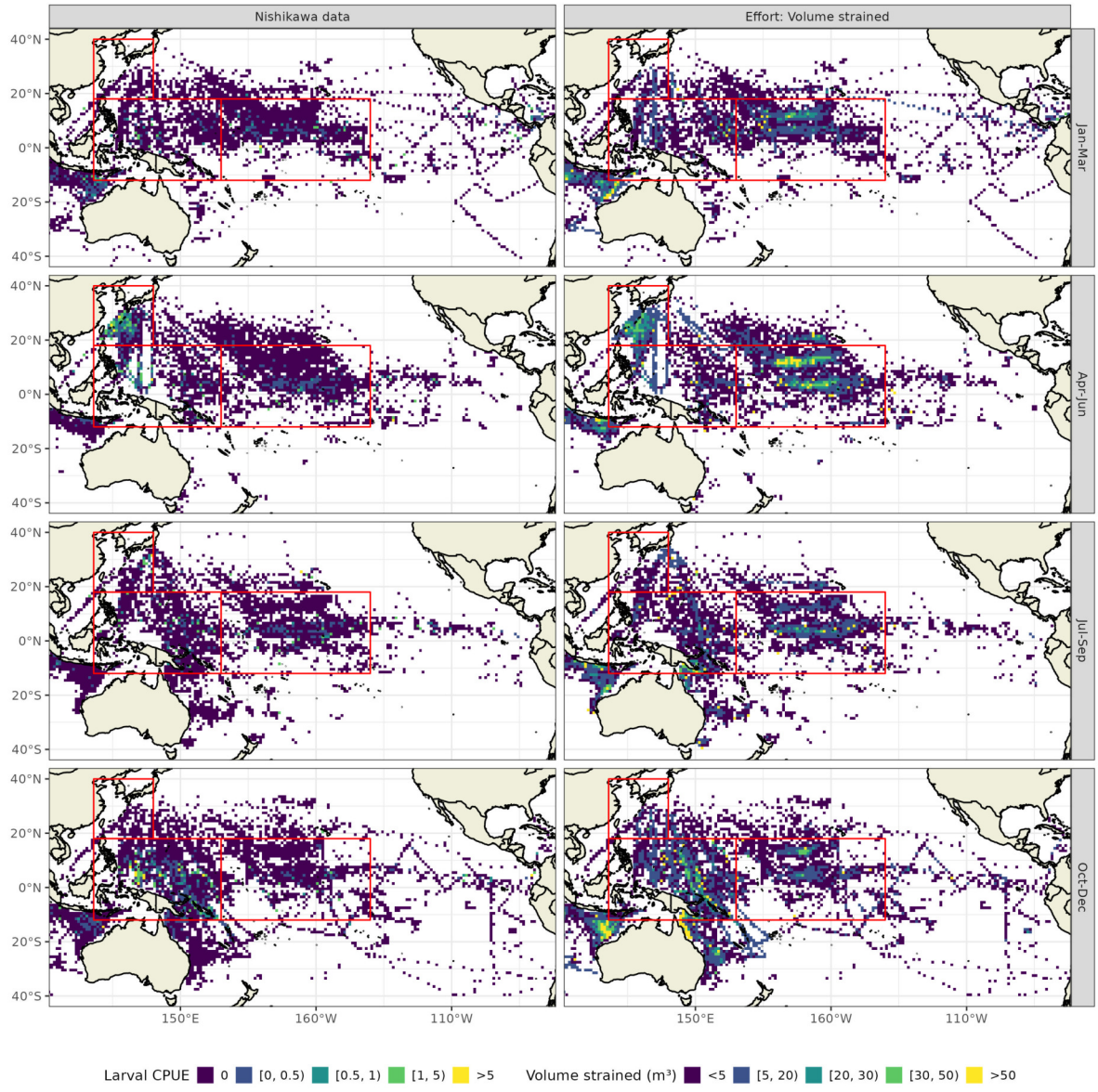

Figure 22: Yellowfin tuna larval CPUE and sampling effort from the Nishikawa dataset.

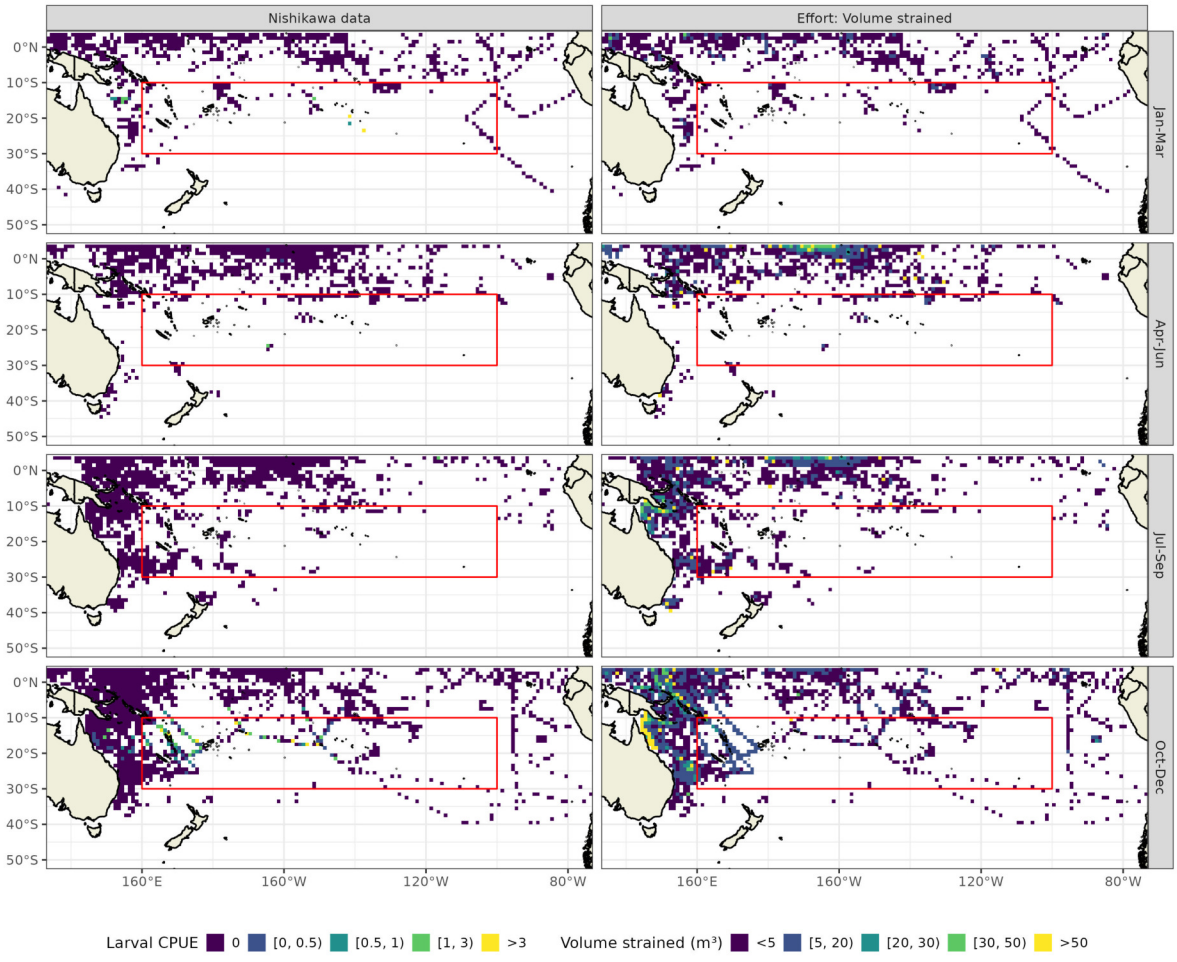

Figure 23: Albacore tuna larval CPUE and sampling effort from the Nishikawa dataset.

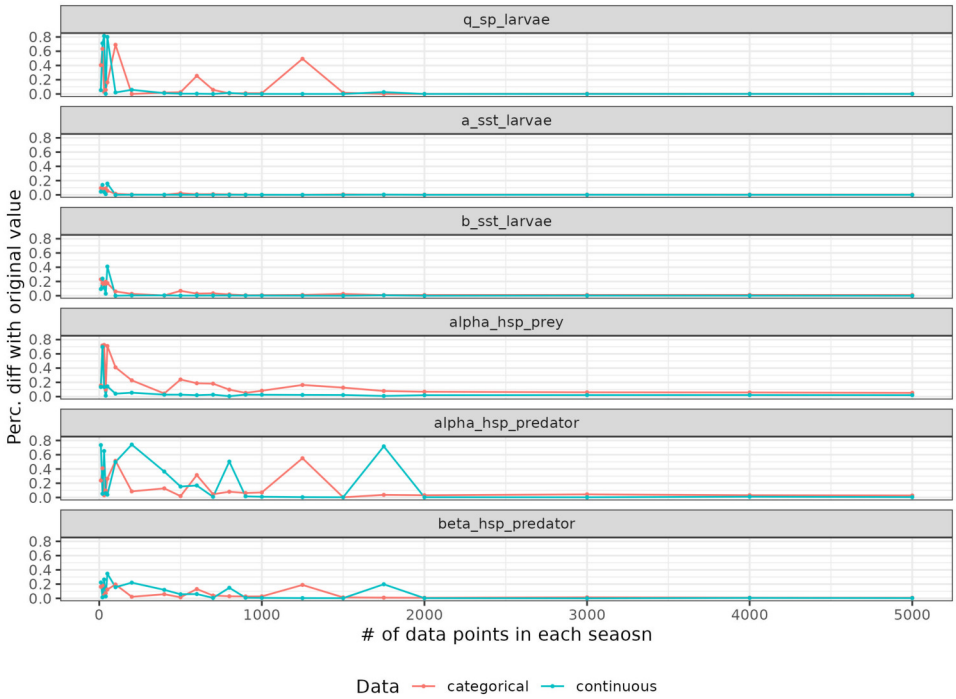

Figure 24: Twin experiments

Figure 25: Outcome of twin experiments using the SEAPODYM habitat model with categorical and continuous data - optimization on the whole set of spawning habitat parameters. An original model with original parameter values was used to generate larval density categorical outputs. Seasonal pseudo-datasets were extracted from these outputs, with varying quantities of randomly sampled grid cells. The ability of the optimization process to estimate parameter values accurately was estimated as the percentage difference to the original parameter values.

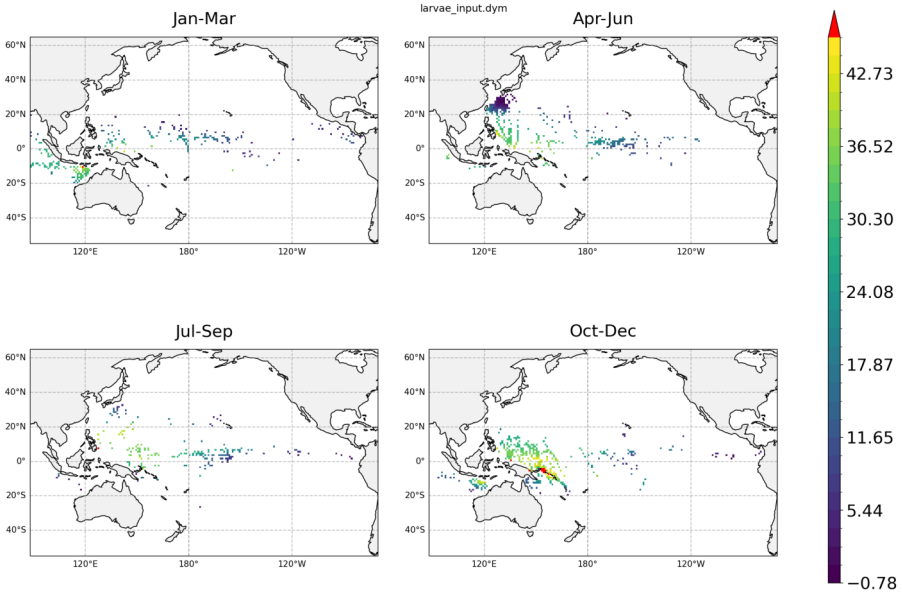

Figure 26: Continuous pseudo-data with same spatial coverage as the Nishikawa dataset, used for twin experiments. Only cells with $N_{obs} > 0$ in the yellowfin tuna Nishikawa dataset were selected here.

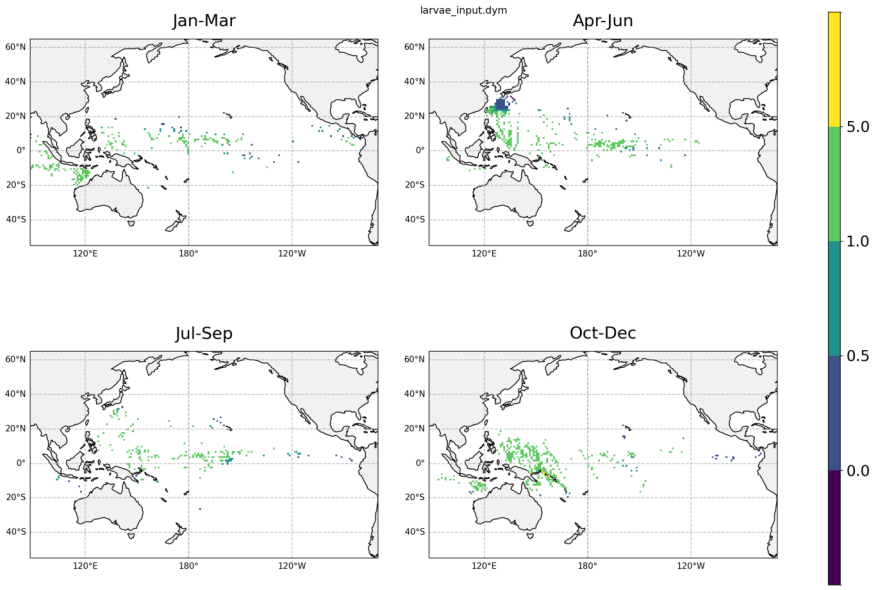

Figure 27: Categorical pseudo-data with same spatial coverage as the Nishikawa dataset, used for twin experiments. Only cells with $N_{obs} > 0$ in the yellowfin tuna Nishikawa dataset were selected here.

(a) Epipelagic micronekton

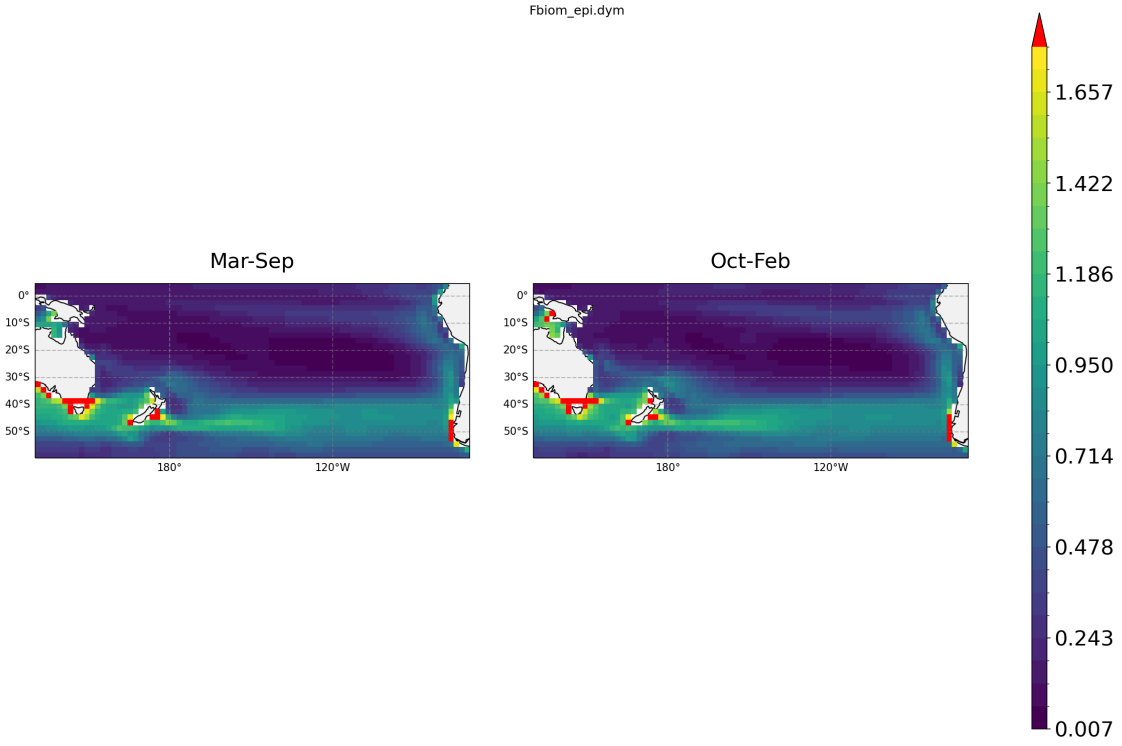

(b) Sea Surface Temperature

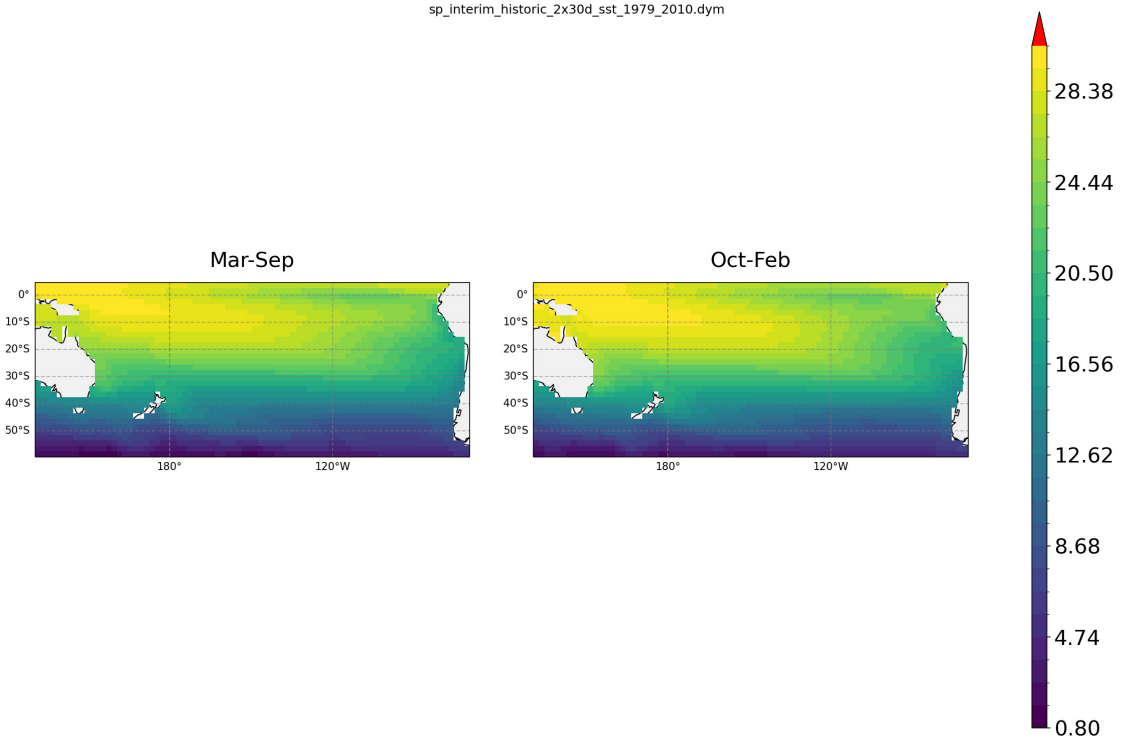

Figure 28: Seasonal variability in environmental forcing involved in the spawning habitat index. A combination of ERA-INTERIM and NEMO-PISCES models were used for environmental forcing.

(c) Primary production

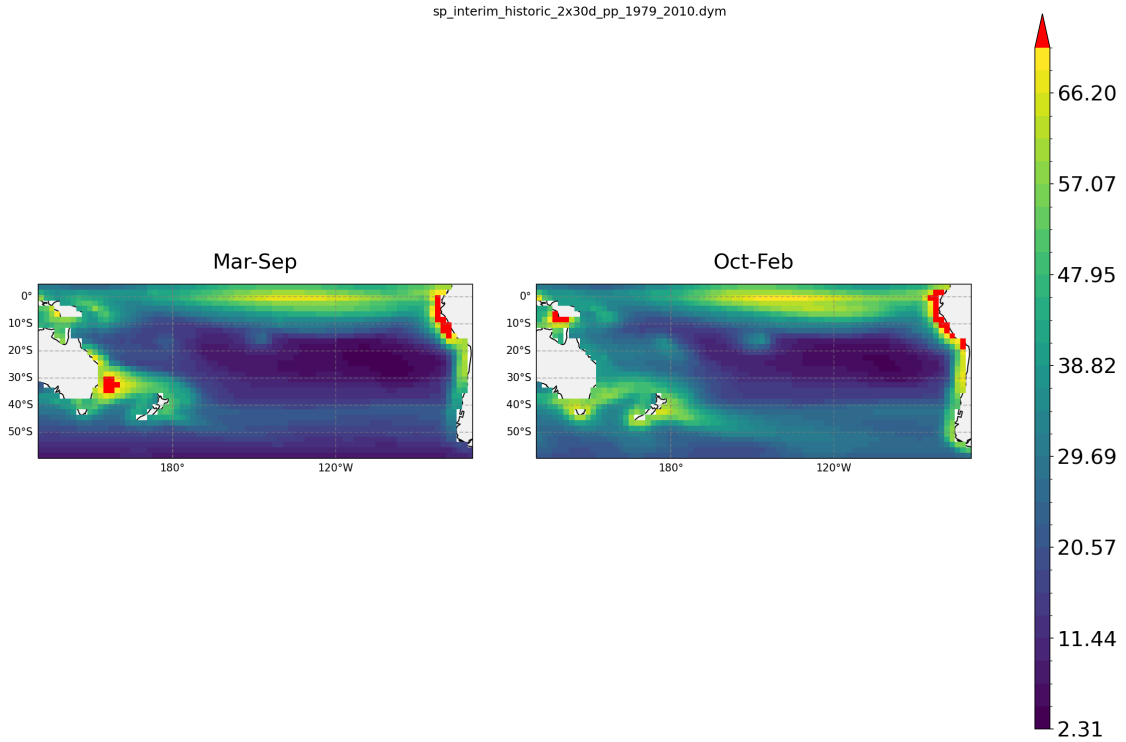

Figure 28: Seasonal variability in environmental forcing involved in the spawning habitat index (Continued).

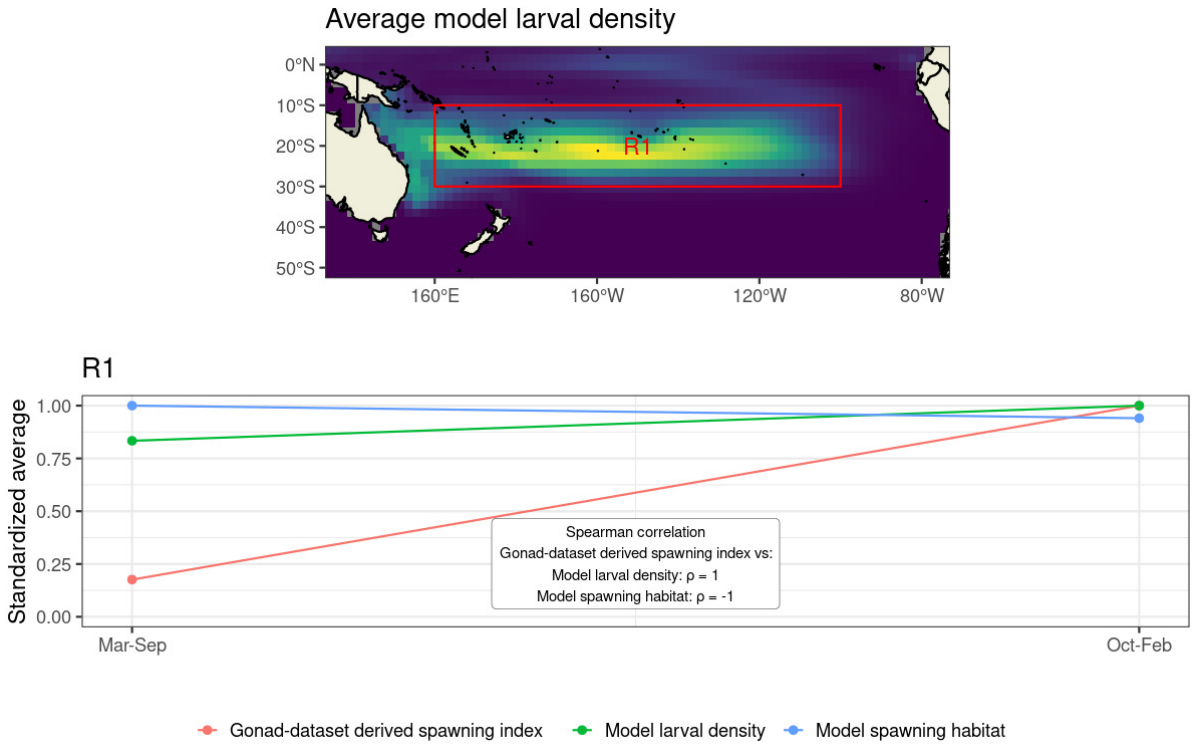

Figure 29: Seasonal variations of albacore tuna gonad data-derived spawning index and reference model outputs. Spawning index and reference model outputs were extracted and averaged in each region and season. For each region, values were standardized by their maximal seasonal value.

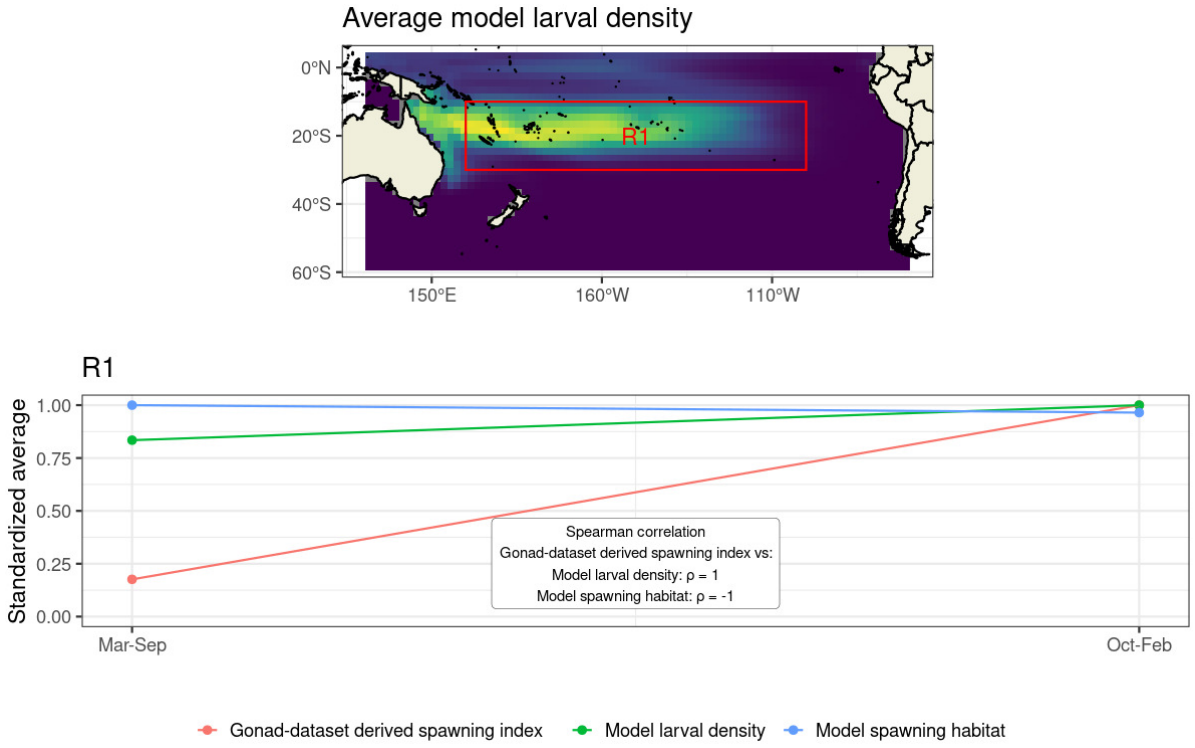

Figure 30: Seasonal variations of albacore tuna gonad data-derived spawning index and re-fitted model outputs. Spawning index and re-fitted model outputs were extracted and averaged in each region and season. For each region, values were standardized by their maximal seasonal value.